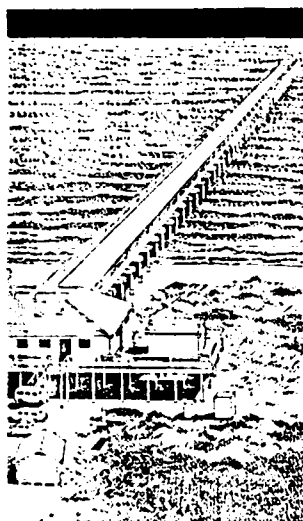


MICROCOPY RESOLUTION TEST CHART
NATIONAL BUREAU OF STANDARDS-1963-A



US Army Corps
of Engineers



DTIC FILE UUF



MISCELLANEOUS PAPER CERC-84-7

12

SPATIAL VARIABILITY IN THE NEARSHORE WAVEFIELD

by

Steven A. Hughes

Coastal Engineering Research Center

DEPARTMENT OF THE ARMY
Waterways Experiment Station, Corps of Engineers
PO Box 631
Vicksburg, Mississippi 39180-0631

AD-A146 907



July 1984

Final Report

Approved For Public Release; Distribution Unlimited

DTIC
ELECTE
OCT 30 1984

B

Prepared for

DEPARTMENT OF THE ARMY
US Army Corps of Engineers
Washington, DC 20314

84 10 23 019

Destroy this report when no longer needed. Do not
return it to the originator.

The findings in this report are not to be construed as an
official Department of the Army position unless so
designated by other authorized documents.

The contents of this report are not to be used for
advertising, publication, or promotional purposes.
Citation of trade names does not constitute an
official endorsement or approval of the use of such
commercial products.

Unclassified

SECURITY CLASSIFICATION OF THIS PAGE (When Data Entered)

REPORT DOCUMENTATION PAGE		READ INSTRUCTIONS BEFORE COMPLETING FORM
1. REPORT NUMBER Miscellaneous Paper CERC-84-7	2. GOVT ACCESSION NO.	3. RECIPIENT'S CATALOG NUMBER
4. TITLE (and Subtitle) SPATIAL VARIABILITY IN THE NEARSHORE WAVEFIELD		5. TYPE OF REPORT & PERIOD COVERED Final report
		6. PERFORMING ORG. REPORT NUMBER
7. AUTHOR(s) Steven A. Hughes		8. CONTRACT OR GRANT NUMBER(s)
9. PERFORMING ORGANIZATION NAME AND ADDRESS US Army Engineer Waterways Experiment Station Coastal Engineering Research Center PO Box 631, Vicksburg, Mississippi 39180-0631		10. PROGRAM ELEMENT, PROJECT, TASK AREA & WORK UNIT NUMBERS
11. CONTROLLING OFFICE NAME AND ADDRESS DEPARTMENT OF THE ARMY US Army Corps of Engineers Washington, DC 20314		12. REPORT DATE July 1984
		13. NUMBER OF PAGES 70
14. MONITORING AGENCY NAME & ADDRESS (if different from Controlling Office)		15. SECURITY CLASS. (of this report) Unclassified
		15a. DECLASSIFICATION/DOWNGRADING SCHEDULE
16. DISTRIBUTION STATEMENT (of this Report) Approved for public release; distribution unlimited.		
17. DISTRIBUTION STATEMENT (of the abstract entered in Block 20, if different from Report)		
18. SUPPLEMENTARY NOTES Available from National Technical Information Service, 5285 Port Royal Road, Springfield, Virginia 22161.		
19. KEY WORDS (Continue on reverse side if necessary and identify by block number) Cross-spectra Wave data Nearshore wavefield Wave height Wave coherence Wave spectra		
20. ABSTRACT (Continue on reverse side if necessary and identify by block number) The Coastal Engineering Research Center, under sponsorship from the Naval Civil Engineering Laboratory, collected wave data for 25 days from a closely spaced array of five wave gages moored in 17 m of water offshore of the North Carolina coast. The objective of the collection was to determine the spatial variability of the wave field under a variety of incident wave conditions to aid the NCEL in planning ship mooring tests. The spatial vari- ability of the wave field was examined in terms of the coherence function (Continued)		

Unclassified

SECURITY CLASSIFICATION OF THIS PAGE(When Data Entered)

20. ABSTRACT (Continued)

measured between pairs of wave gages. The primary factor affecting the coherence function is the spatial separation between the gages. Coherence was found to rapidly decrease as spatial separation increased, particularly in the along-crest direction (right-angle to the direction of wave travel). The effect of spatial separation was quantified as nondimensional coherence contours which provide a first rough estimate of the wave coherence which would be expected between two gages.

Unclassified

SECURITY CLASSIFICATION OF THIS PAGE(When Data Entered)

SUMMARY

The Coastal Engineering Research Center (CERC), under sponsorship from the Naval Civil Engineering Laboratory (NCEL), collected wave data for 25 days from a closely spaced array of five wave gages moored in 17 m of water offshore of the North Carolina coast. The objective of the collection was to determine the spatial variability of the wave field under a variety of incident wave conditions to aid the NCEL in planning ship mooring tests. The spatial variability of the wave field was examined in terms of the coherence function measured between pairs of wave gages. The primary factor affecting the coherence function is the spatial separation between the gages. Coherence was found to rapidly decrease as spatial separation increased, particularly in the along-crest direction (right-angle to the direction of wave travel). The effect of spatial separation was quantified as nondimensional coherence contours which provide a first rough estimate of the wave coherence which would be expected between two gages. Because of the approximate nature of the estimation technique, collection of onsite coherence data is recommended for future field exercises if such data are needed for subsequent analyses. As a result of this research, some operational recommendations are provided to aid in conducting future ship mooring experiments. These recommendations are as follows:

- Align the two wave gages parallel with the central incident wave direction.
- Maintain equal scope on all wave gage moorings.
- Relocate wave buoys when possible to maintain the desired alignment with the wave field.
- Place additional vacant buoy moorings in an array to facilitate buoy relocation.
- Moor a backup wave buoy at the experimental site.
- Avoid data collection during times when the wave energy is concentrated at the higher frequencies and during the presence of multiple wave trains approaching from different directions.

Accession For

NTIS GRA&I

DTIC TAB

Unannounced

Justification _____

By _____

Distribution/ _____

Availability Codes

Dist	Avail and/or Special
A-1	

PREFACE

This investigation was performed by the Coastal Engineering Research Center (CERC) of the US Army Engineer Waterways Experiment Station (WES), Vicksburg, Miss., as requested by the Department of the Navy, Naval Civil Engineering Laboratory (NCEL), Port Hueneme, California.

The study was conducted under the direction of Dr. R. W. Whalin, Chief, CERC, Mr. R. P. Savage, former Chief, Research Division, Dr. J. R. Houston, Chief, Research Division, Dr. C. L. Vincent, former Chief, Coastal Oceanography Branch, and Dr. E. F. Thompson, Chief, Coastal Oceanography Branch. The report was prepared by Dr. Steven A. Hughes, Hydraulic Engineer, who also served as technical coordinator. Computer analyses of the data were performed by Ms. J. M. McKee and Mr. S. C. Wheeler.

The field measurement portion of this study was performed by the staff of CERC's Field Research Facility (FRF), in particular, Mr. E. W. Bichner, Mr. W. E. Grogg, Mr. M. W. Leffler, Mr. C. R. Townsend, and Mr. S. C. Wheeler, under the supervision of Mr. C. Mason, Chief.

The Project Monitor for the Naval Civil Engineering Laboratory was Mr. Paul Palo.

Commander and Director of WES during the conduct of this investigation and the preparation of the report was COL Tilford C. Creel, CE. Technical Director was Mr. F. R. Brown.

CONTENTS

	<u>Page</u>
SUMMARY	1
PREFACE	2
PART I: INTRODUCTION	4
Background	4
Objective of the Experiment	4
PART II: DATA COLLECTION	5
Wave Gages	5
Data Collected	5
PART III: DATA ANALYSIS	8
PART IV: RESULTS	12
Classification in Terms of Incident Wave Direction	12
Coherence Trends	12
Spatial Variability	12
Coherence Contours	16
Analytical Phase Shift	20
PART V: SUMMARY AND RECOMMENDATIONS	27
REFERENCES	31
TABLES 1-2	
APPENDIX A: COHERENCE PLOTS	A1

SPATIAL VARIABILITY IN THE NEARSHORE WAVEFIELD

PART I: INTRODUCTION

Background

1. The Naval Civil Engineering Laboratory (NCEL) is investigating ship motions and mooring forces for vessels anchored in coastal waters. A mooring force model has been developed by NCEL, but field data are required in order that NCEL can verify the model's accuracy and determine its limitations. In the NCEL model, the wave field is to be applied at the center of gravity of the ship. Since this is an artificial constraint, i.e., there are no waves at this point, it is desirable to estimate the differences between the waves causing ship motion and those a few hundred feet away where wave data can be collected without excessive ship-induced interference. Naturally occurring waves are not long-crested and the waves change in form as they propagate. Since the form of each wave striking the ship is important, field studies for verifying the mooring force model could be planned more effectively if the following information were available: (a) the best position to locate a gage to record wave data suitable for evaluating mooring response, and (b) the variation in wave form that can be expected between the recorded waves and those which actually cause the ship motion.

2. To help meet this need for information, the Coastal Engineering Research Center (CERC) collected data for 25 days at the Field Research Facility (FRF) at Duck, North Carolina, under NCEL sponsorship. Five Waverider wave measuring buoys were moored in proximity to each other, and wave data were collected simultaneously from all gages.

Objective of the Experiment

3. The primary objective was to obtain time series records of the sea surface displacements for periods of wind-generated seas, swell, and for the case when more than one distinct wavetrain was present. Determining the spatial variability of the wavefield in both the along-wave and the cross-wave directions was the primary aim of the data analysis.

PART II: DATA COLLECTION

Wave Gages

4. Between 23 April and 10 June 1983, wave data were collected from an array of five Datawell Waverider wave gages moored in a depth of 17 m. The array was positioned about 2 km offshore of the FRF (Figure 1). The dimensions and orientation of the Waverider array, as shown in Figure 2, were determined after placement using a land-based laser surveying instrument during calm wave conditions. All the buoys in the array were tethered to mooring lines of the same scope with the intent that any displacement due to a unidirectional current would result in a translation of the array with minimum distortion. There was variation in the array dimensions and orientation to a limited extent due to wave-induced displacements of the buoys, but these spatial differences averaged out over the period of data collection.

5. Prior to deployment all the Waveriders were calibrated according to the manufacturer's recommendations using a Ferris wheel arrangement. All the gages met or exceeded the calibration specification required by Datawell. A posttest check of the calibration curves for two CERC buoys used in the experiment indicated that the calibration error for these two was less than 4 percent.

Data Collected

6. The data set was comprised of 38 data collection sessions lasting 80 min each. These are summarized in Table 1. Data were obtained for periods of wind-generated seas, swell, and for cases when more than one distinct wave-train was present. Each session involved the simultaneous recording of wave data from all gages at a sampling rate of four points per second resulting in a total record of 19,200 data points per gage. The collection sessions (runs) were substantially longer than normal because it was realized a unique data set was being collected and that the longer records might be very useful for future analyses. The raw data were collected at the FRF on a Data General Nova-4 computer and stored on magnetic tape.

7. The wave direction for each recording session was routinely obtained using the X-band radar at the FRF, supplemented by visual observations.

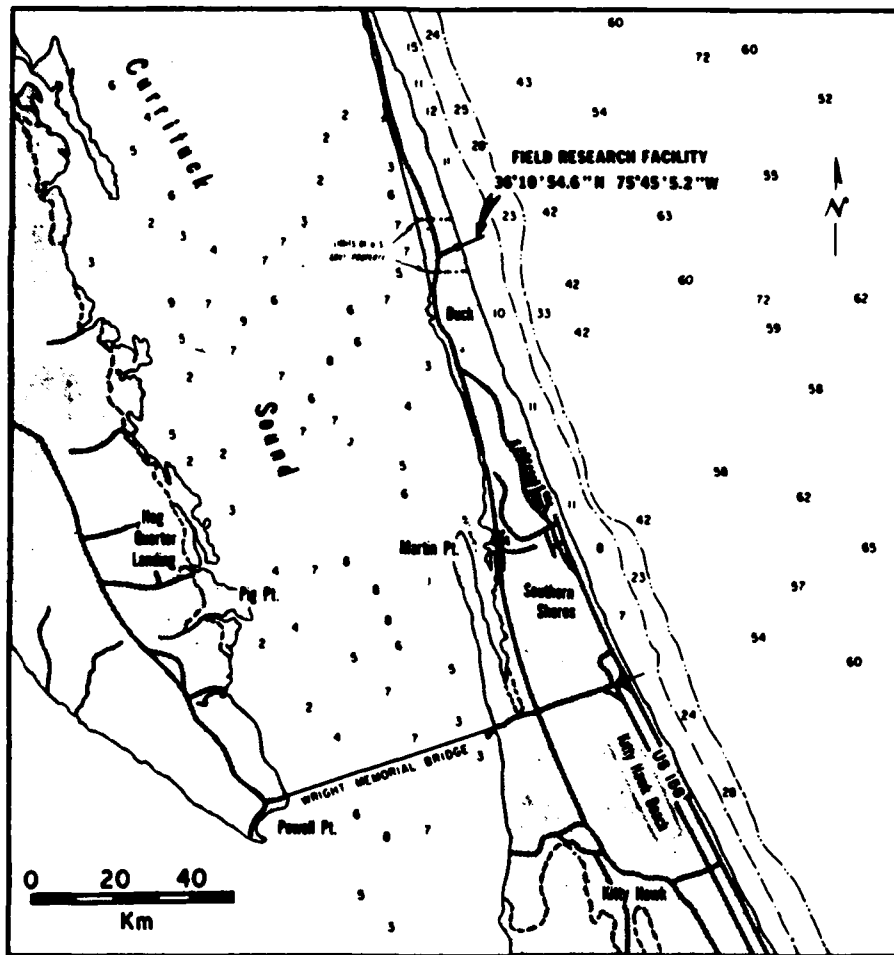
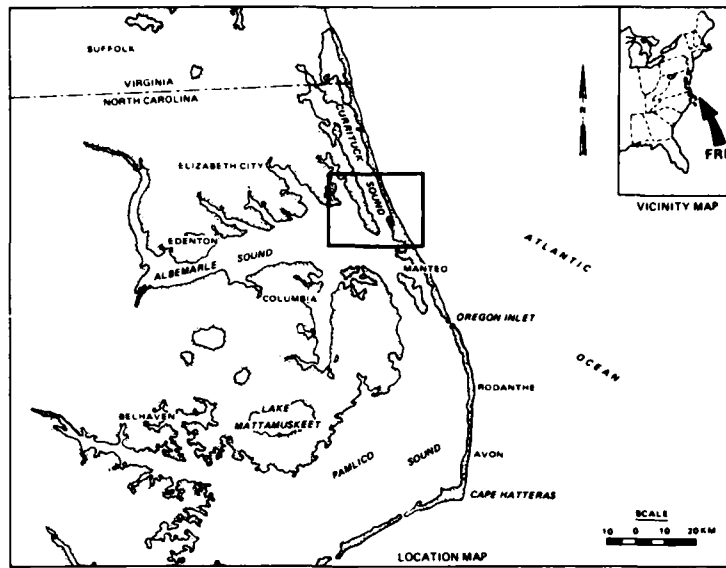


Figure 1. Field research facility location map

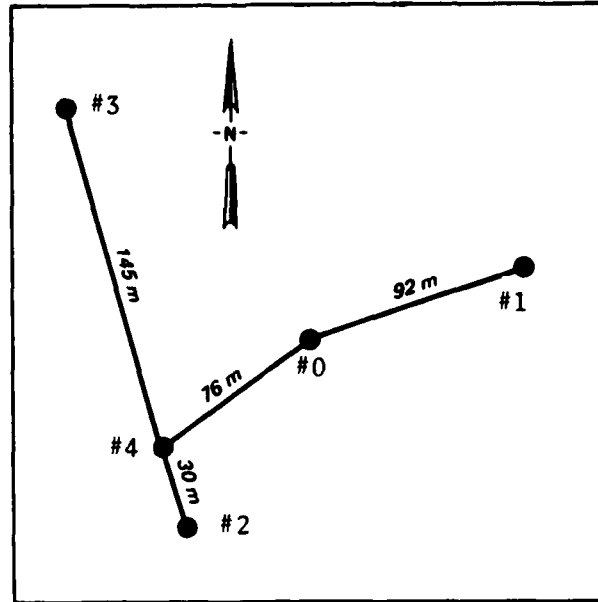


Figure 2. Waverider wave gage array

Mattie and Harris (1979) report the direction measuring capability of the Doppler radar to be accurate to within ± 4 percent. In cases with two distinct wavetrains approaching from different directions, the directions of both primary and secondary wavetrains were recorded. Pertinent weather data were noted during each recording session, and aerial photographs of the wave field were obtained several times over the duration of the experiment.

8. The most southerly Waverider buoy (see Figure 2) produced erratic results from the onset of the experiment and was replaced as soon as possible. Consequently, the data from the first 22 collection runs do not include data from this buoy. Runs after run 22 include results from the most southerly gage in the array.

PART III: DATA ANALYSIS

9. Nine of the data collection runs were selected for analysis, as indicated in Table 1, and represent a fairly broad range of conditions. Further details of the analysis subset are provided in Table 2.

10. The analysis for each run consisted of determining the energy density spectrum for each gage and performing cross-spectral analysis to determine wave coherence and phase functions from data gathered between all possible gage pairings. The coherence function between two spatially separated time series of ocean waves measures the extent to which the time series at one position can be predicted from the wave field at the other position, assuming a linear dependence exists between the two. By definition the coherence function is given as

$$\gamma_{xy}(f) = \frac{|G_{xy}(f)|}{[G_{xx}(f)G_{yy}(f)]^{1/2}} \quad (1)$$

where

$G_{xy}(f)$ = cross-spectral density function between gages X and Y

$G_{xx}(f)$ = autospectral density function of gage X

$G_{yy}(f)$ = autospectral density function of gage Y

The coherence values are bounded between zero (no relation between the positions) and a coherence of one (complete linear dependence). The coherence function rapidly decreases as the distance between the two spatial positions increases. This is one reason that ocean waves are more often described in terms of energy spectra with parameters relating the spectra between locations.

11. The first five analysis runs resulted in six possible pairings of gages per run due to the malfunctioning of the most southerly Waverider. The remaining four runs each contain 10 possible pairings. In all instances only every other data point in the first 2048 sec of the recorded time series was used in the data analysis subset. Thus the analysis subset contains 4096 points sampled at 0.5-sec time intervals. This provides a sufficient number of points to insure accurate representation of the spectra in the frequency range 0.05 to 1.0 Hz (1- to 20-sec wave periods) without becoming overly burdensome for analysis. There is evidence that coherence estimates are not appreciably improved by increasing the length of the time series beyond 2048 data points (Briggs 1981). In fact, a long data set could introduce questions

about stationarity of the wave field during the recording interval.

12. The data were processed with a Fast Fourier Transform (FFT) routine. The resolution in the frequency domain is 0.0004883 Hz. Since frequencies higher than 0.25 Hz (4 sec) are considered to be of little practical importance and since the coherences at these high frequencies are expected to be very small, attention was concentrated on the frequencies ranging from 0 to 0.25 Hz. The analysis produced spectral values at 512 discrete frequencies in this frequency range.

13. Gages were paired for cross-spectral analysis, and cross-spectral energy densities were computed. A Tukey filter was applied to the cross-spectrum Fourier coefficients to increase the statistical stability of the results with only a minor loss in resolution. Coherence and phase were computed from the smoothed cross-spectral values.

14. It would have been possible to time shift one time series with respect to the other time series of the wave gage pairing in an attempt to improve the coherence. This was not done for several reasons. First, there is a difficulty in selecting an appropriate time shift for each pairing. A possible candidate would be the time it takes the wave associated with the peak of the spectrum to traverse the distance between gages. However, this lag time will vary for each gage and doesn't fully compensate for all the waves traveling at different speeds. Second, the amount of wave record not overlapped in time (based on the travel time of the peak period wave) never exceeded 1.5 percent of the total record and most often this percentage was much less. While not actually tested, it was believed that time shifting one record with respect to another would not significantly alter the coherence, and it would have the disadvantage of introducing an additional questionable assumption into the analysis.

15. Coherence values greater than 0.7 (coherence-squared values greater than about 0.5) are considered to indicate a meaningful coherence between signals, although admittedly this is a rather arbitrary demarcation. The analyses were searched for coherence values greater than 0.7. Fifty percent of the cross-spectral analysis indicated such coherences in at least part of the frequency range. The cases which did not have any coherence values above 0.7 represented pairing of the gages which had large spatial separation (particularly in the along-crest direction) for the incident wave direction. For all cases with reasonably high coherence, the coherence function and the

autospectral energy density functions were plotted, as illustrated in Figure 3. The entire set of plots is given in Appendix A. For plotting purposes the discrete frequency intervals were combined into 100 bands by averaging every five values. This had only a minor smoothing effect on the plotted results.

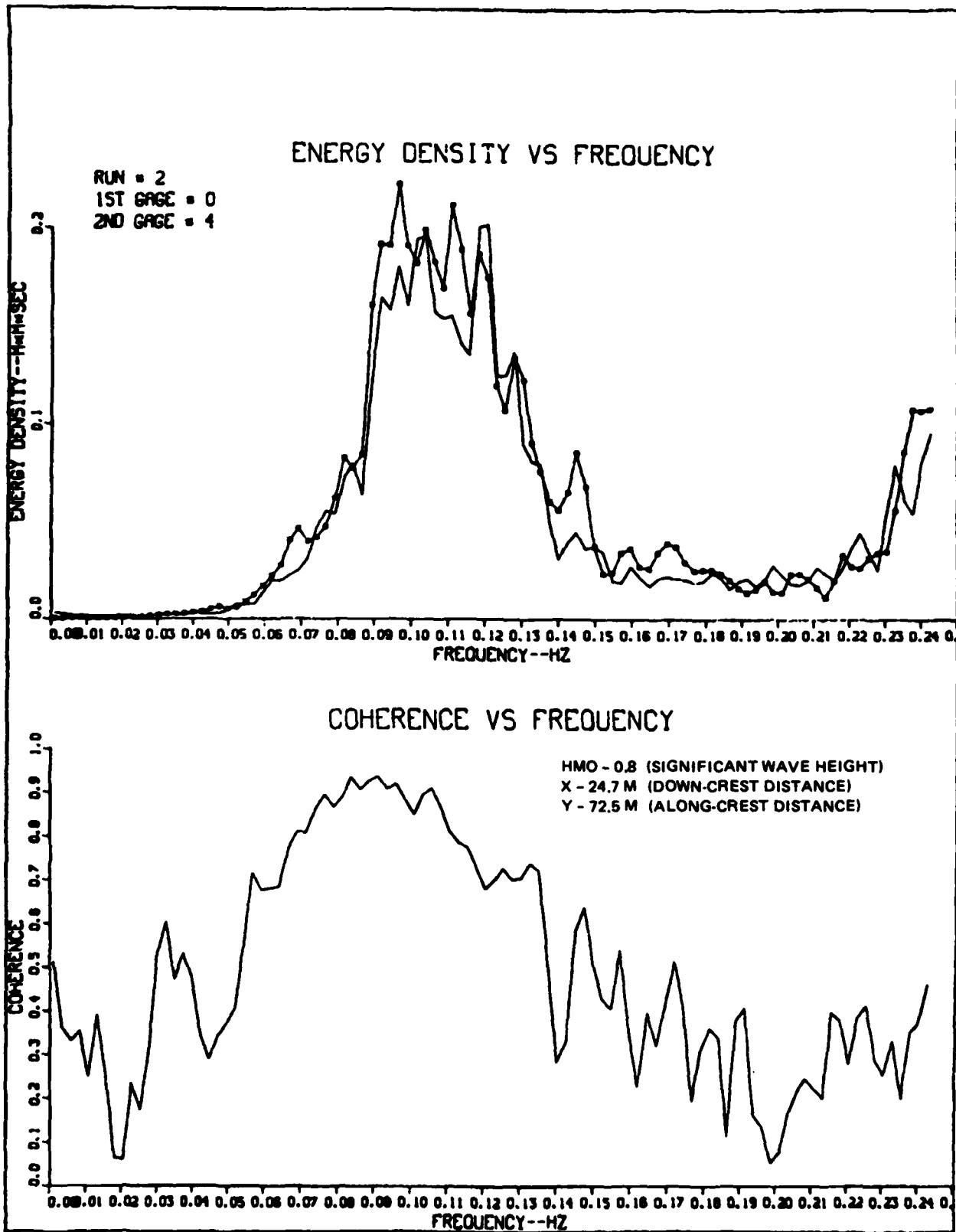


Figure 3. Example of the Appendix A wave spectra and coherence plots

PART IV: RESULTS

Classification in Terms of Incident Wave Direction

16. For every incident wave direction, the vector distance between each wave gage pairing can be resolved into a component parallel to the wave crests and a component perpendicular to the crests as illustrated by Figure 4. This breakdown provides a means of assessing spatial variability in the wave field. The "along-crest" distance has been labeled as Y, and the "down-crest" distance as X on the plots of coherence in Appendix A. Both X and Y are expressed in meters. Values of X and Y are given for both the primary and the secondary directions when two distinct wave trains were present (see Figure 4). HMO on the plots is equal to four times the standard deviation of sea surface elevations in meters, but is commonly referred to as significant wave height. The gage numbers of the pairing used for the plot refer to the Wave-rider numbering as shown in Figure 2.

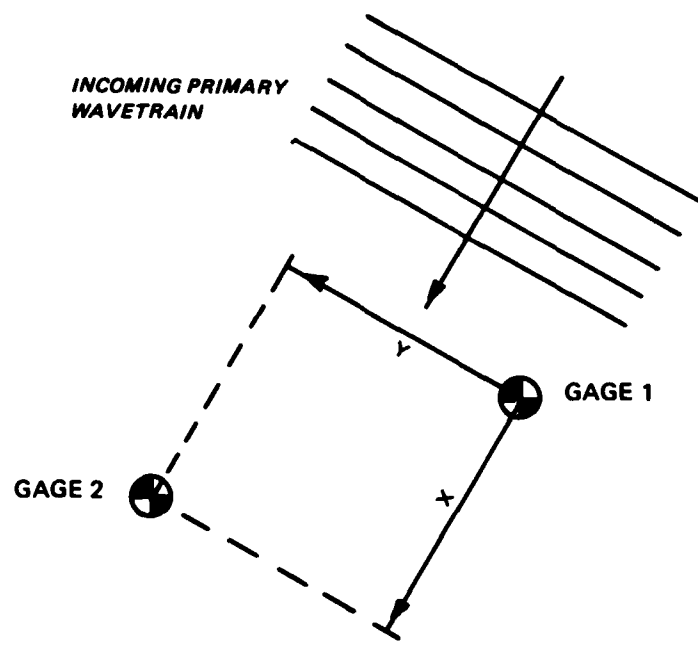
Coherence Trends

17. Several qualitative trends are observed in the plots in Appendix A. The coherence function is weakly, if at all, dependent upon the shape of the spectrum or the amount of energy contained in the spectrum. For example, the two plots given in Figure 5 show coherence functions which are quite similar even though the spectra between run 3 and run 7 are considerably different. Run 3 represents a narrow spectrum while run 7 is a broad spectrum with the energy spread over a wide range of frequencies.

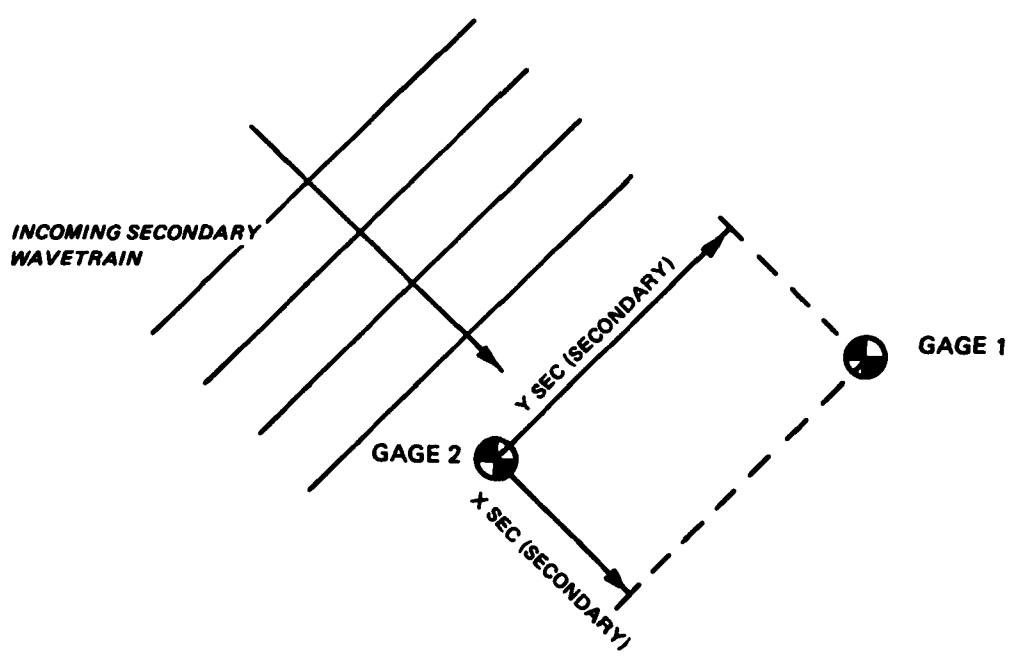
18. The coherence function does not appear to be influenced greatly by the width of the spectral peak or by the frequency at which it is located. The region of good coherence for run 3 in Figure 5 is considerably wider than the peak of the spectrum. Run 6 (Figure 6) represents spectra with peak frequencies higher than those in Figure 5 but with a very similar coherence function.

Spatial Variability

19. The most apparent influence on the coherence function is understandably the spatial separation of the buoys. The coherence plots in



a. Primary wave direction



b. Secondary wave direction

Figure 4. Definition of along-crest and down-crest distances

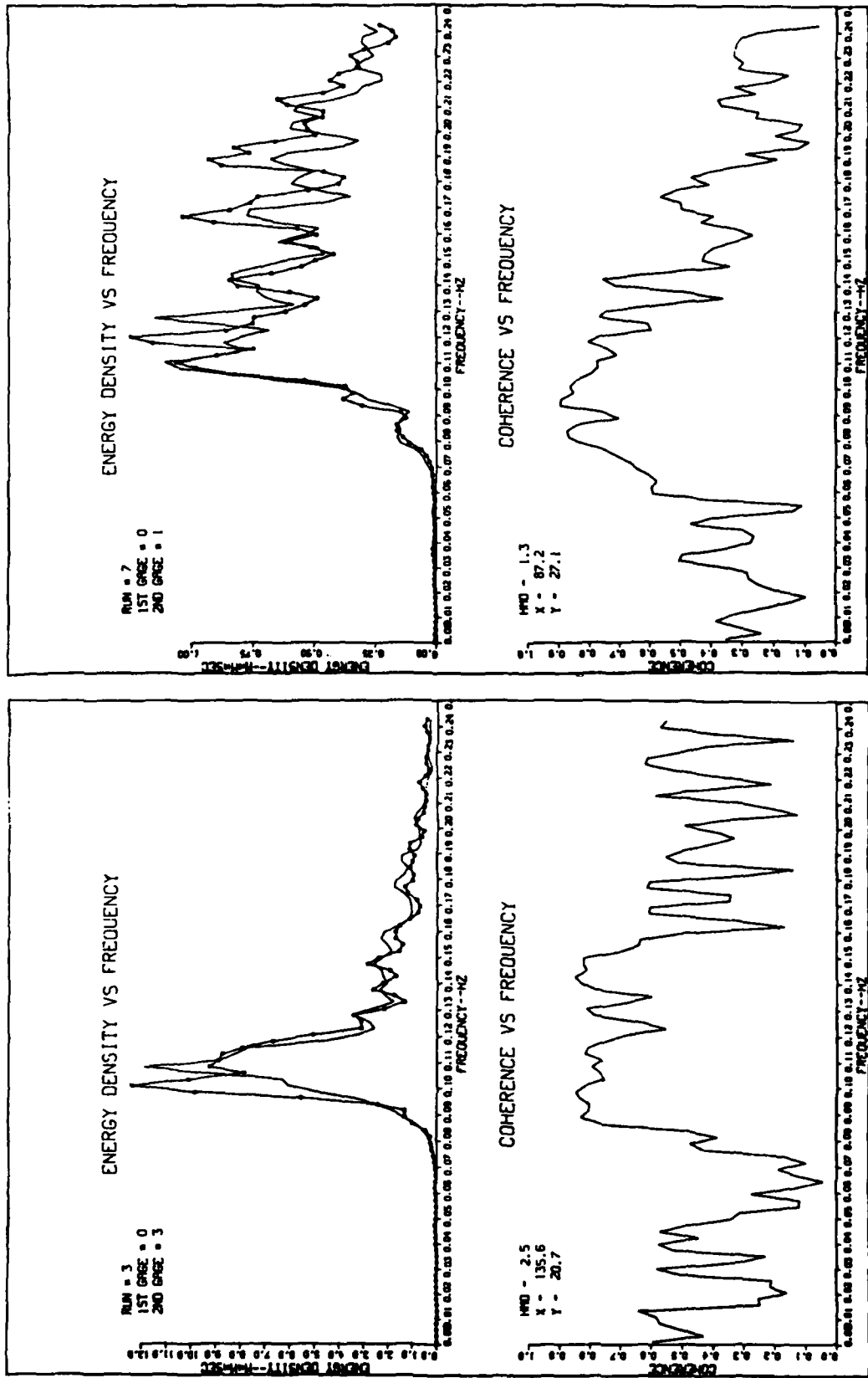


Figure 5. Comparison of coherence results, runs 3 and 7

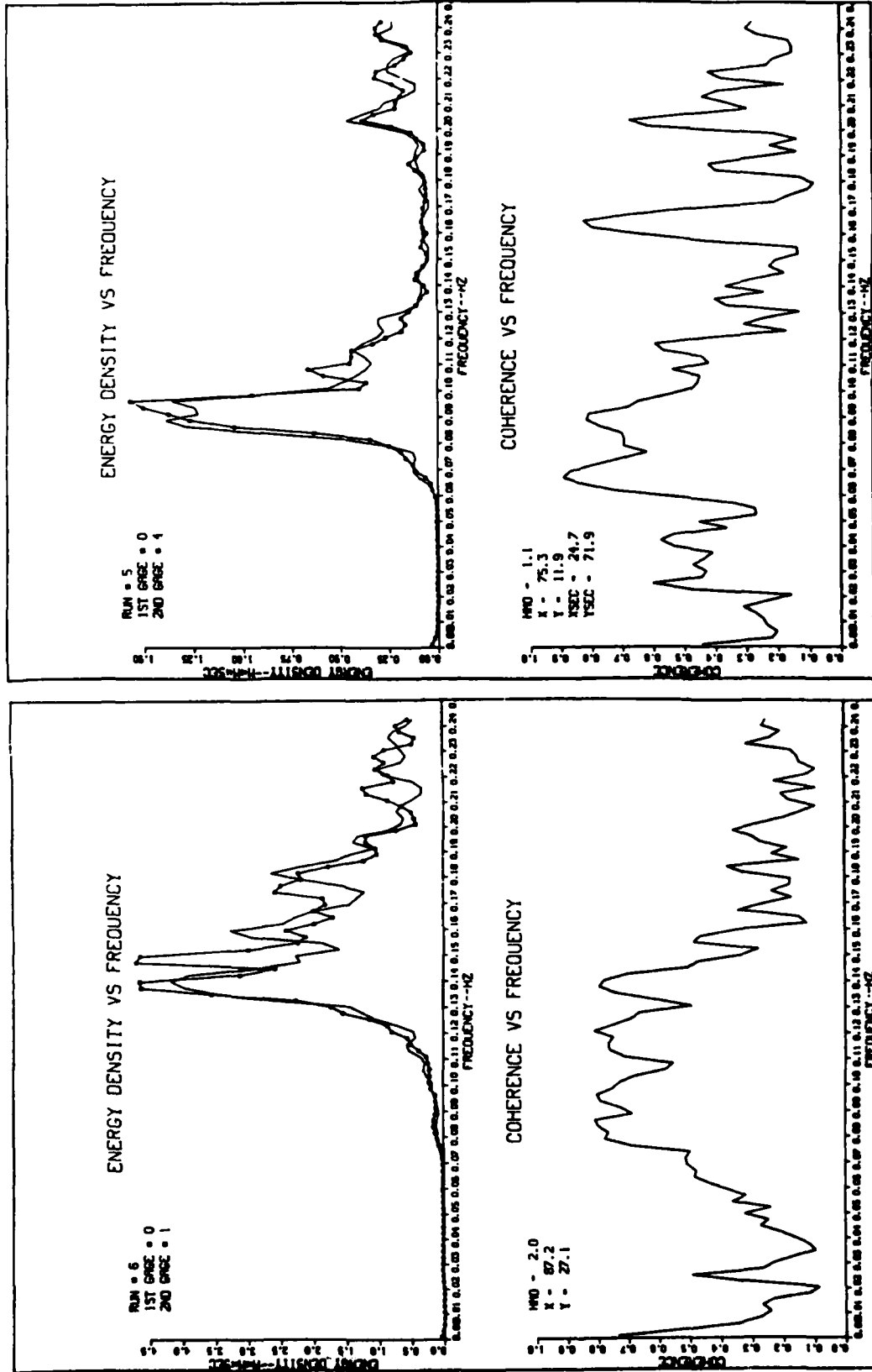


Figure 6. Comparison of coherence results, runs 6 and 5

Appendix A have been arranged in order of increasing along-crest (Y) separation distances. The trend is a decrease in coherence, particularly in the higher frequencies, as the along-crest separation distance increases, sometimes regardless of the down-crest (X) separation. While the down-crest distance has some influence, the overall variation in coherence function is more closely tied to the along-crest distance than to any other single parameter. A convenient way to represent this "short-crestedness" is to nondimensionalize the along-crest (Y) and the down-crest (X) distances by the wavelength (L) associated with each frequency in 17-m water depth. All discrete values of coherence can then be plotted against the separation distance in terms of relative wavelength.

20. To illustrate the importance of the along-crest separation versus the down-crest separation, plots were made using all discrete coherence values between 0.078 and 0.16 Hz, which covers the range of meaningful coherence and the principal energy-containing frequencies in nearly all cases. Figure 7 gives coherence versus the nondimensional along-crest distance for all values except the multiwavetrain cases, and Figure 8 contains the same coherences as a function of nondimensional down-crest distance. A tendency for coherence to decrease more rapidly with increasing along-crest separation than with increasing down-crest separation is evident in the figures. The line shown in Figure 7 could represent an approximate upper limit boundary to the coherence data. Up to values of Y/L around 1.5, the curve is probably a good estimate of the best possible coherence which could be obtained between two gages aligned parallel to the wave crests. A similar upper limit curve is drawn in Figure 8, but the plotted values of coherence are more evenly distributed between zero and one than those in Figure 7. Thus the upper limit line in Figure 8 is less well defined. These upper limit curves should be considered only in conjunction with spatial separations on the order of 30 m or more.

21. Attempts were made to examine the data as a function of the magnitude of the separation vector and the angle of orientation of the vector with respect to the incident waves. Qualitatively, the data followed the expected trends but the scatter was far too wide to justify any quantitative treatment.

Coherence Contours

22. A nondimensional plot of coherence contours is given in Figure 9.

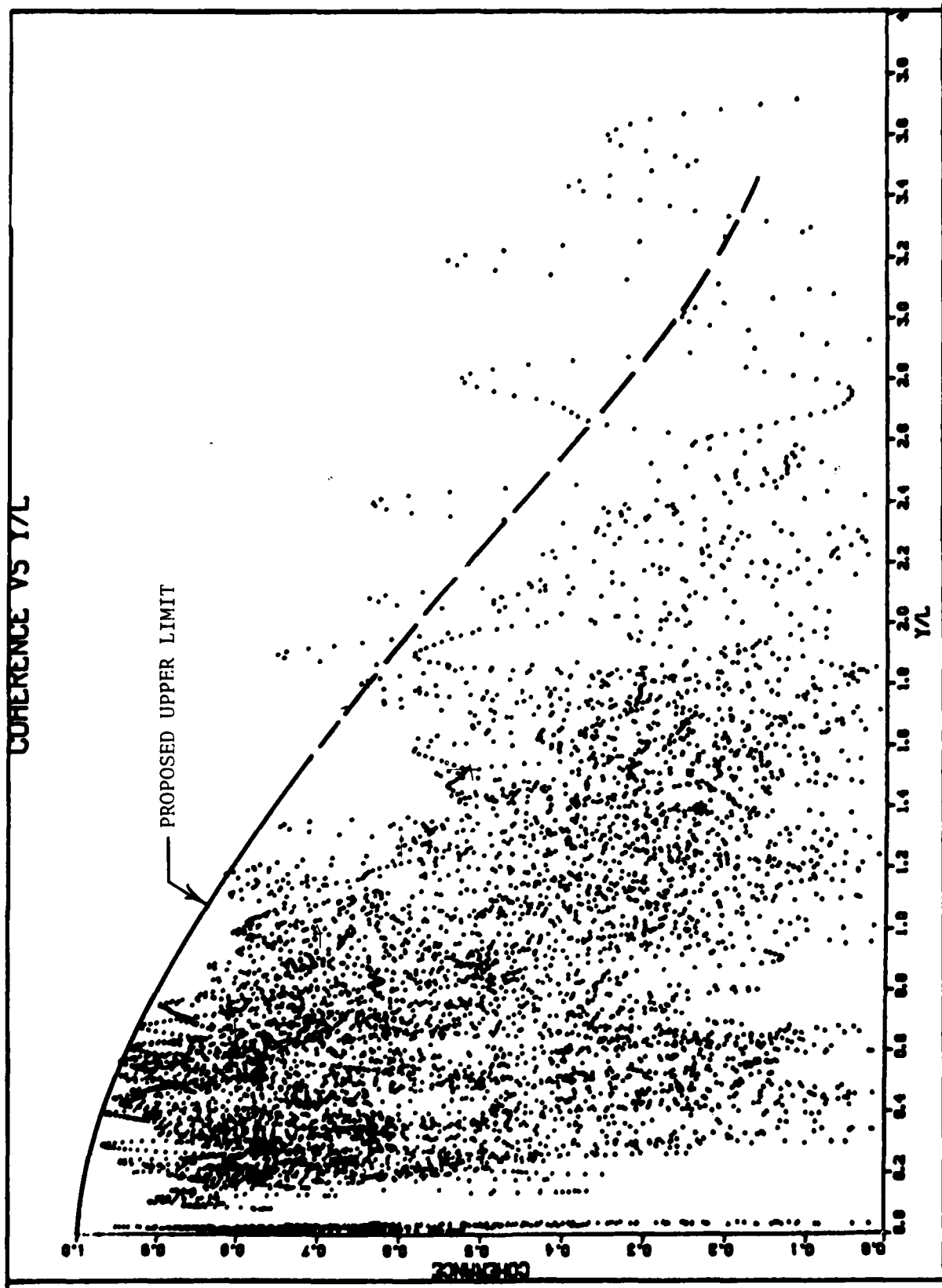


Figure 7. Coherence versus nondimensional along-crest separation

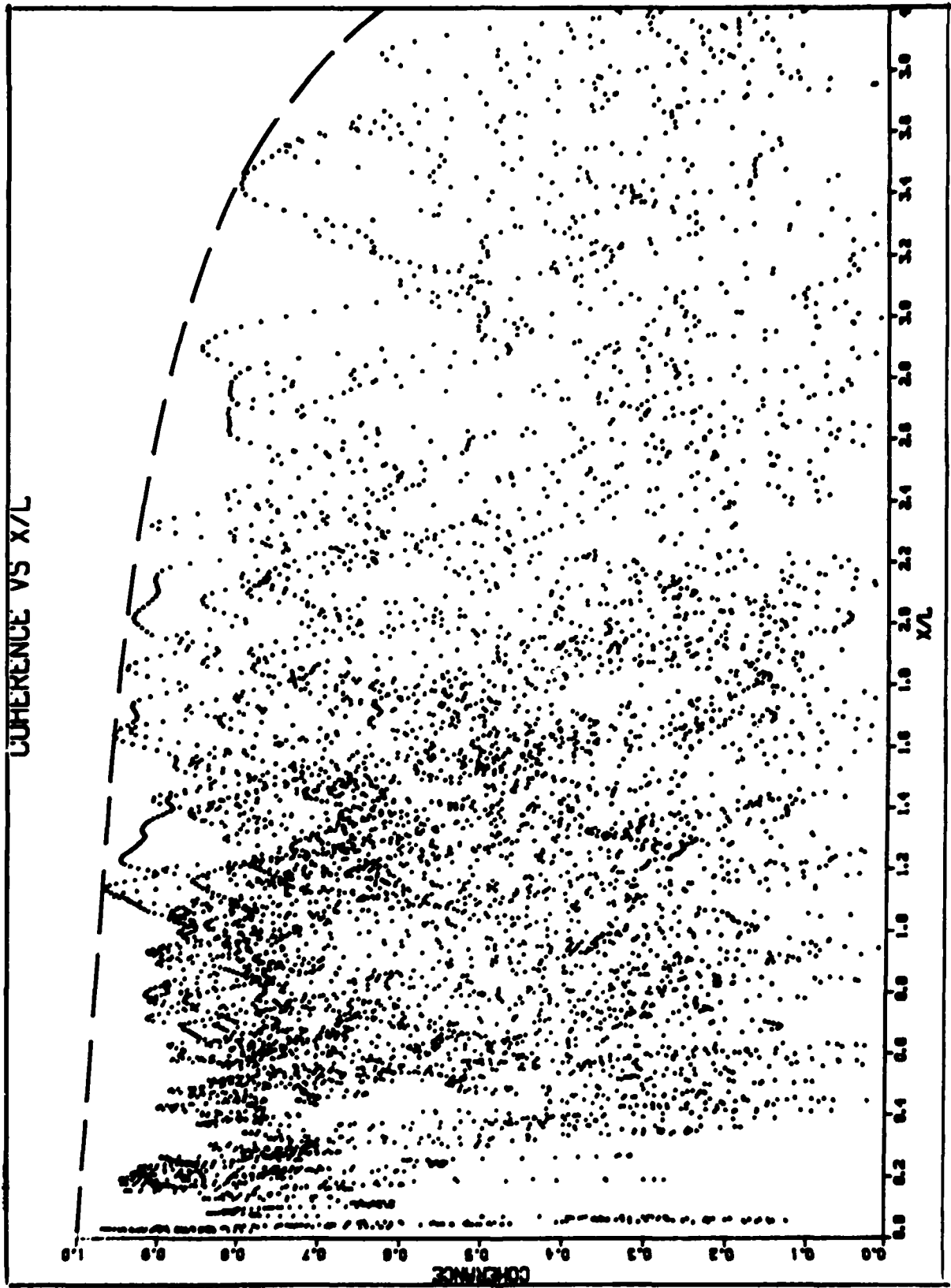


Figure 8. Coherence versus nondimensional down-crest separation

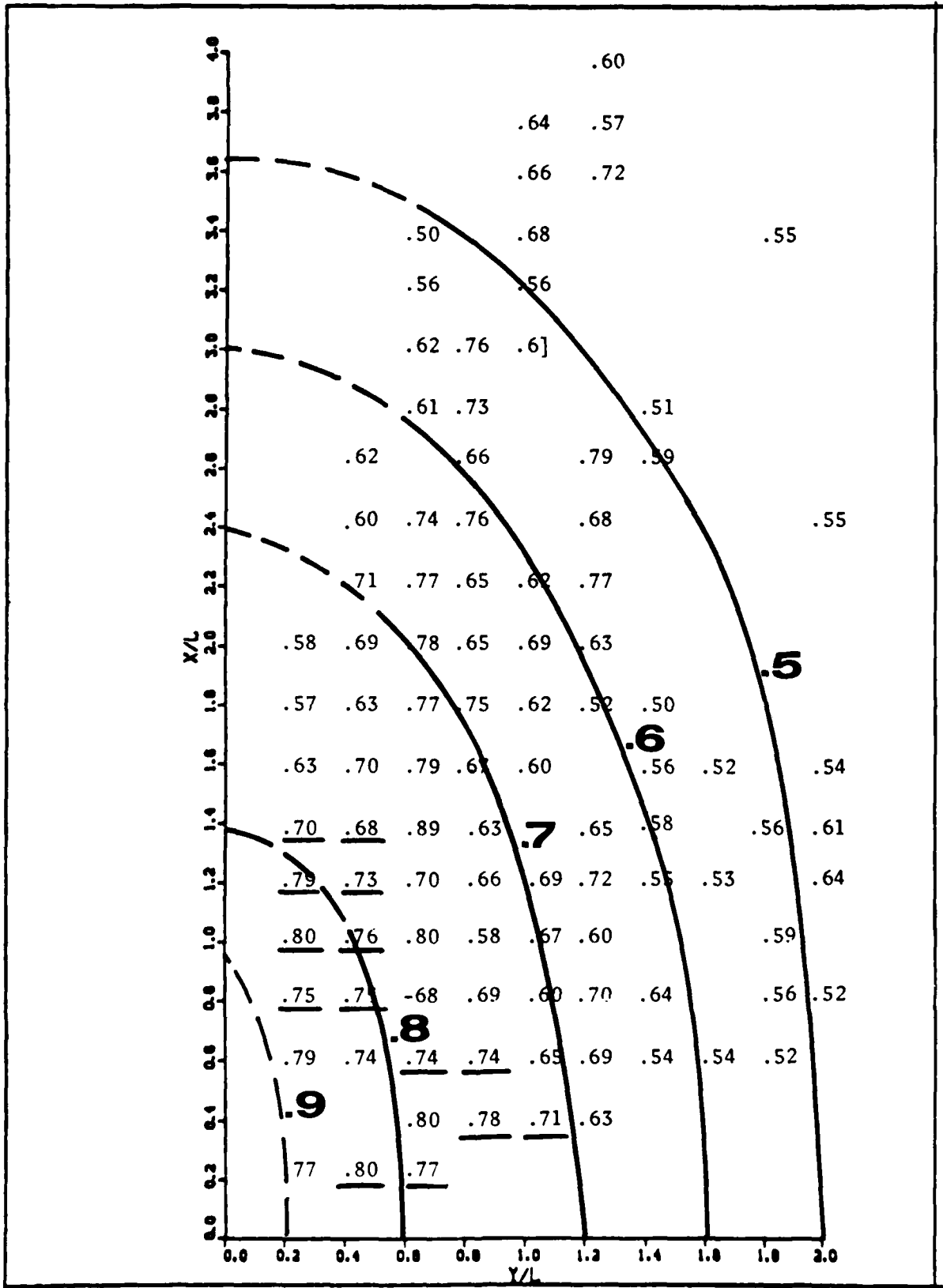


Figure 9. Nondimensional coherence contours for shallow water (17 m)

The horizontal axis gives the along-crest separation distance (Y) divided by the wavelength (L) associated with each frequency (linear theory), while the vertical axis gives the nondimensional down-crest separation (X/L). The numerical values on the plot are the average of all discrete values of coherence which fell into 0.2 by 0.2 squares centered on the decimal points on the plot. The underlined values represent the squares containing more than 100 points in the average, and the dashed sections of the contours are surmised. The number of coherence values used in obtaining each average was subjectively considered when sketching the contours. The multiwavetrain data were not included in this formulation; thus, the contours are intended for a wave field approaching from a single central direction.

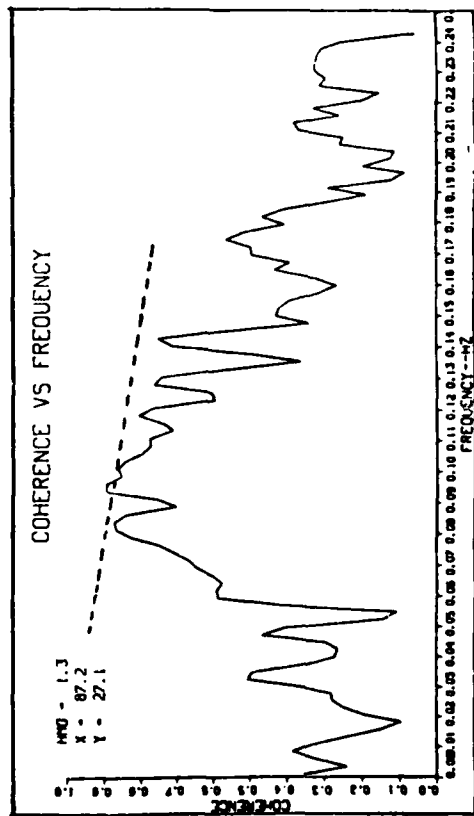
23. The contours are a crude estimate at best since they consider only the spatial separation parameters of a complex process. However, they do provide a means of getting a first estimate of the coherence function between two gage locations. The Y - and X -axis intercept values of the contour lines in Figure 9 are somewhat less than values obtained from the upper limit lines in Figures 7 and 8 because the intercept values are meant to represent average values instead of upper limit values.

24. To illustrate the use of the contours, four coherence plots from Appendix A were chosen, and an estimate of coherence was made using the contours of Figure 9. These results are shown as dashed lines in Figure 10. The estimates are fair in the region of highest coherence, but fail to give satisfactory reproduction at the higher frequencies. It should again be noted that only the frequency range 0.078 to 0.16 Hz was considered in preparing the contours.

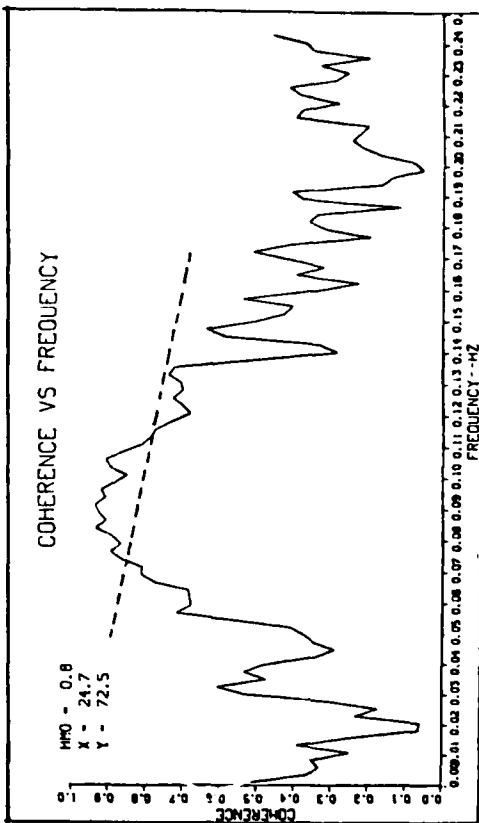
25. It must be emphasized that the results which were contoured in Figure 9 were obtained in a water depth of 17 m. The contours may be useful at other shallow water depths because of the nondimensionalization by wavelength; however, more data are needed to support this generalization.

Analytical Phase Shift

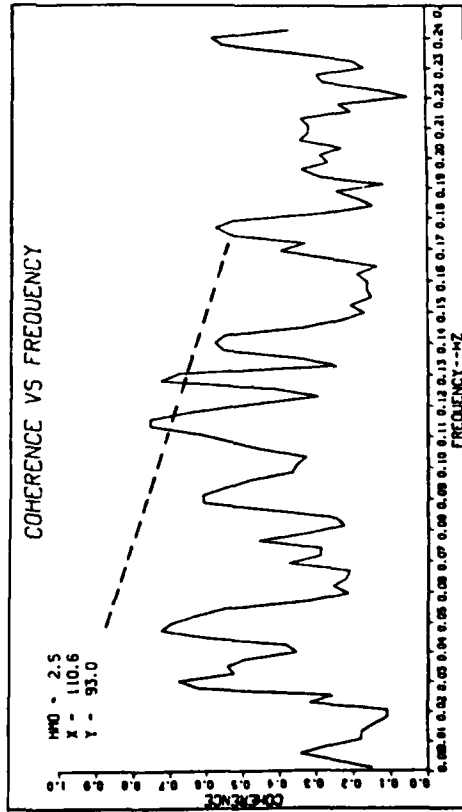
26. An analytical experiment aimed at obtaining improved coherence between two wave gages was performed on three gage pairs. These pairings were selected because they came the closest to having one gage situated directly down-crest of the other gage in the pair. In other words, the "along-crest"



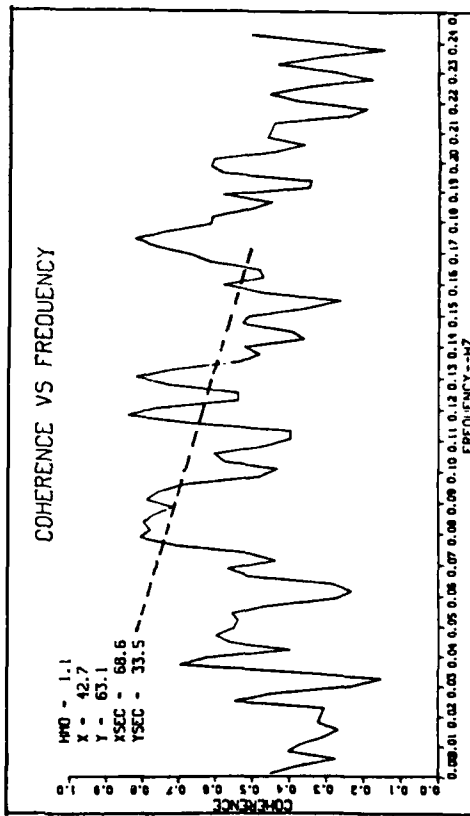
Run #7



Run #2



Run #3



Run #8

Figure 10. Coherence estimates, runs 7, 2, 3, and 8

distance was minimal. The experiment consisted of deterministically translating the upwind wave gage results to the downwind gage position using the linear dispersion relation. It was hoped this would compensate for the fact that waves at different frequencies travel at different speeds. A coherence function could then be determined between the downwind gage and the phase-shifted results from the upwind gage. Then a comparison could be made with the original coherence results to see if any improvement in coherence could be realized. A successful experiment would allow an improved estimate of the wavetrain at a location based on wave data collected a short distance away.

27. The phase shifting was accomplished by modifying the upwind gage Fourier coefficients obtained from the FFT. For each discrete frequency ω a pair of Fourier coefficients, $P_1(\omega)$ and $Q_1(\omega)$, are obtained. They relate to the wave spectrum through the following equations:

$$F_1(\omega) = P_1(\omega) + iQ_1(\omega) = |F_1(\omega)| e^{i\theta_1(\omega)} \quad (2)$$

where

$$|F_1(\omega)| = \sqrt{P_1^2(\omega) + Q_1^2(\omega)} = \text{discrete component of the amplitude spectrum} \quad (3)$$

$$\theta_1(\omega) = \tan^{-1} \left[\frac{Q_1(\omega)}{P_1(\omega)} \right] = \text{discrete component of the phase spectrum} \quad (4)$$

It was assumed for the experiment that the phase angle at the downwind position would be

$$\theta_2(\omega) = \theta_1(\omega) + \Delta\theta(\omega) \quad (5)$$

Since the phase angle can be expressed as

$$\theta(\omega) = \omega t + kx \quad (6)$$

with

ω = circular frequency

t = time

x = downwind spatial distance

k = wave number associated with the frequency ω using linear theory
the spatial correction to the phase angle for $t = \text{constant}$ becomes

$$\frac{\Delta\theta(\omega)}{\Delta x} = k \quad \text{or} \quad \Delta\theta(\omega) = k\Delta x \quad (7)$$

where Δx is the spatial separation of the wave gages.

28. To implement this phase it is necessary at each frequency to determine a new set of Fourier coefficients giving the new phase angle without changing the amplitude, i.e.,

$$\theta_2(\omega) = \theta_1(\omega) + k\Delta x = \tan^{-1} \left[\frac{Q_2(\omega)}{P_2(\omega)} \right] \quad (8)$$

and

$$|F_2(\omega)| = \sqrt{P_2^2(\omega) + Q_2^2(\omega)} = |F_1(\omega)| \quad (9)$$

Thus the new coefficients become

$$P_2(\omega) = |F_1(\omega)| \cos [\theta_1(\omega) + k\Delta x] \quad (10)$$

$$Q_2(\omega) = |F_1(\omega)| \sin [\theta_1(\omega) + k\Delta x] \quad (11)$$

29. Figures 11, 12, and 13 display the results of this experiment with the analytically shifted coherence given by the dashed line. Obviously, the concept is not a workable scheme in reality. A possible source of the difficulty is the use of the linear dispersion relationship.

30. A more probable cause for the failure of the above-mentioned phase modification lies with the phase spectra resulting from the FFT. Although the phase spectra produced by the FFT can be combined with the corresponding amplitude spectra to recover the original time series, it has been demonstrated by Thompson (1982) that phase spectra from FFT analyses may not be a true representation of the phases associated with the physical process being analyzed. Phase spectra from FFT analyses are characterized by large variations between adjacent frequencies. Thompson's research showed that these fluctuations can be induced by limitations of the FFT analysis and are thus partial artifacts of the procedure itself. The fluctuations appear to be a consequence of representing the physical process by a finite number of discrete frequency components. Therefore, modification of an FFT-produced phase spectra is likely to be unsuccessful.

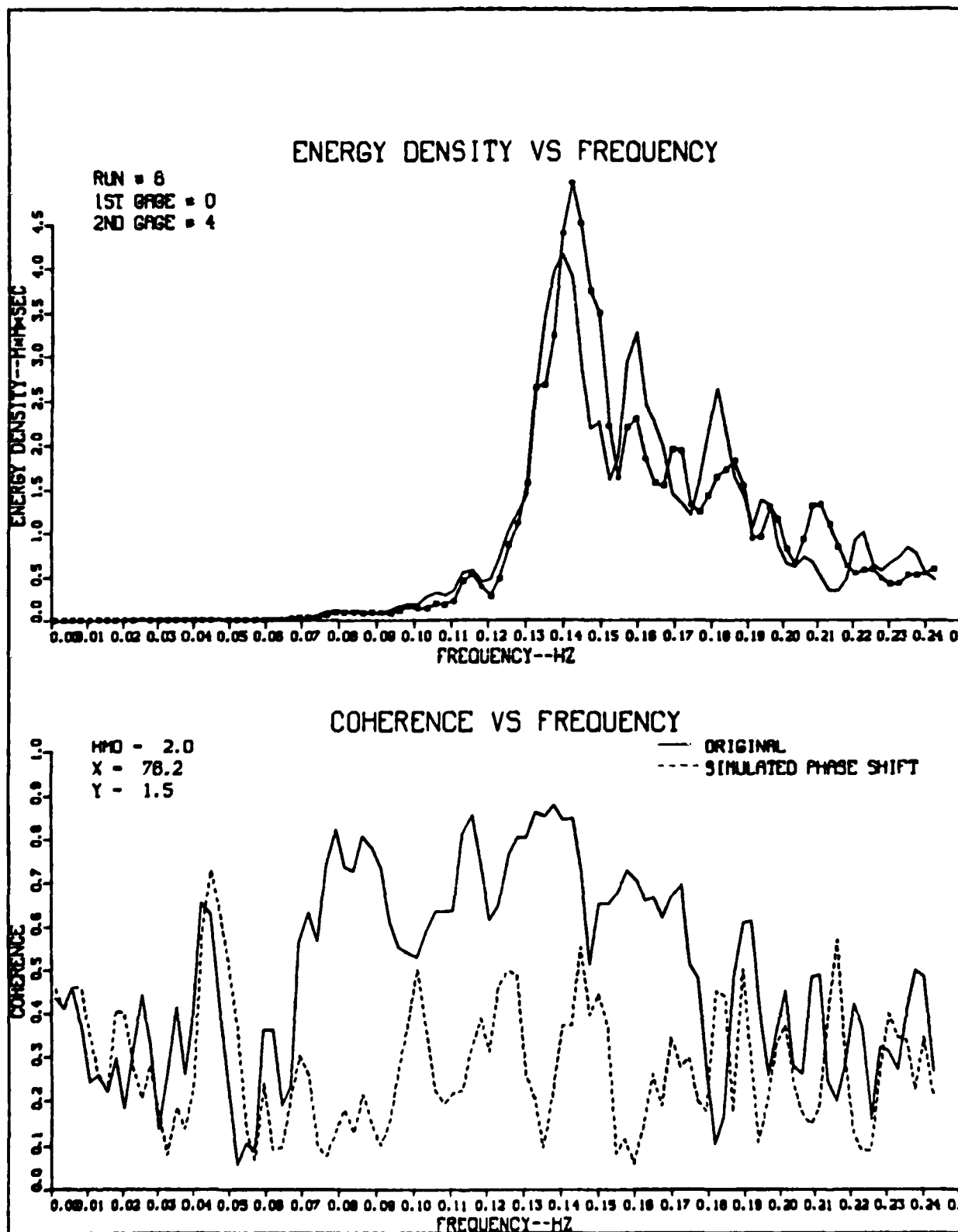


Figure 11. Phase shifted coherence, run 6

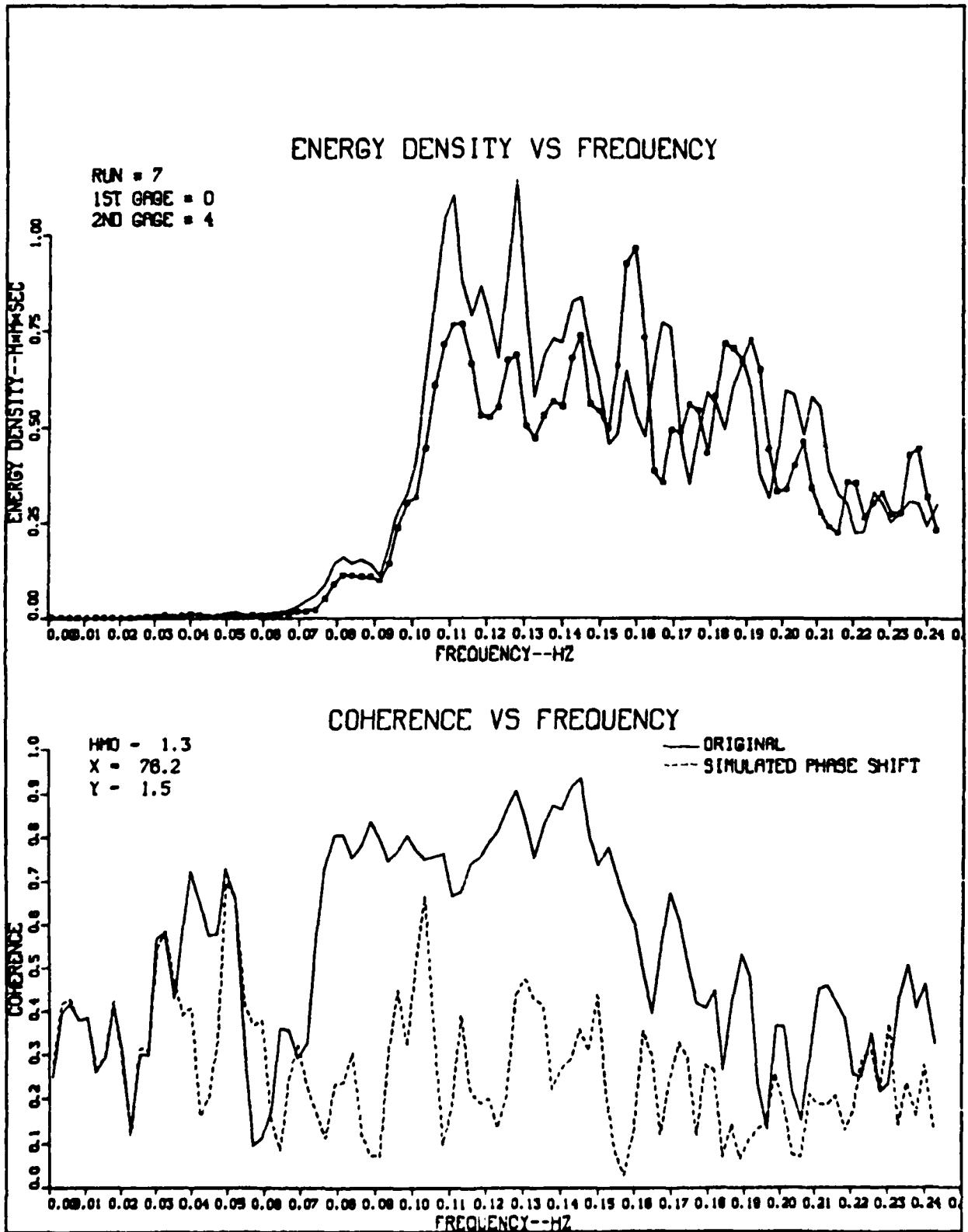


Figure 12. Phase shifted coherence, run 7

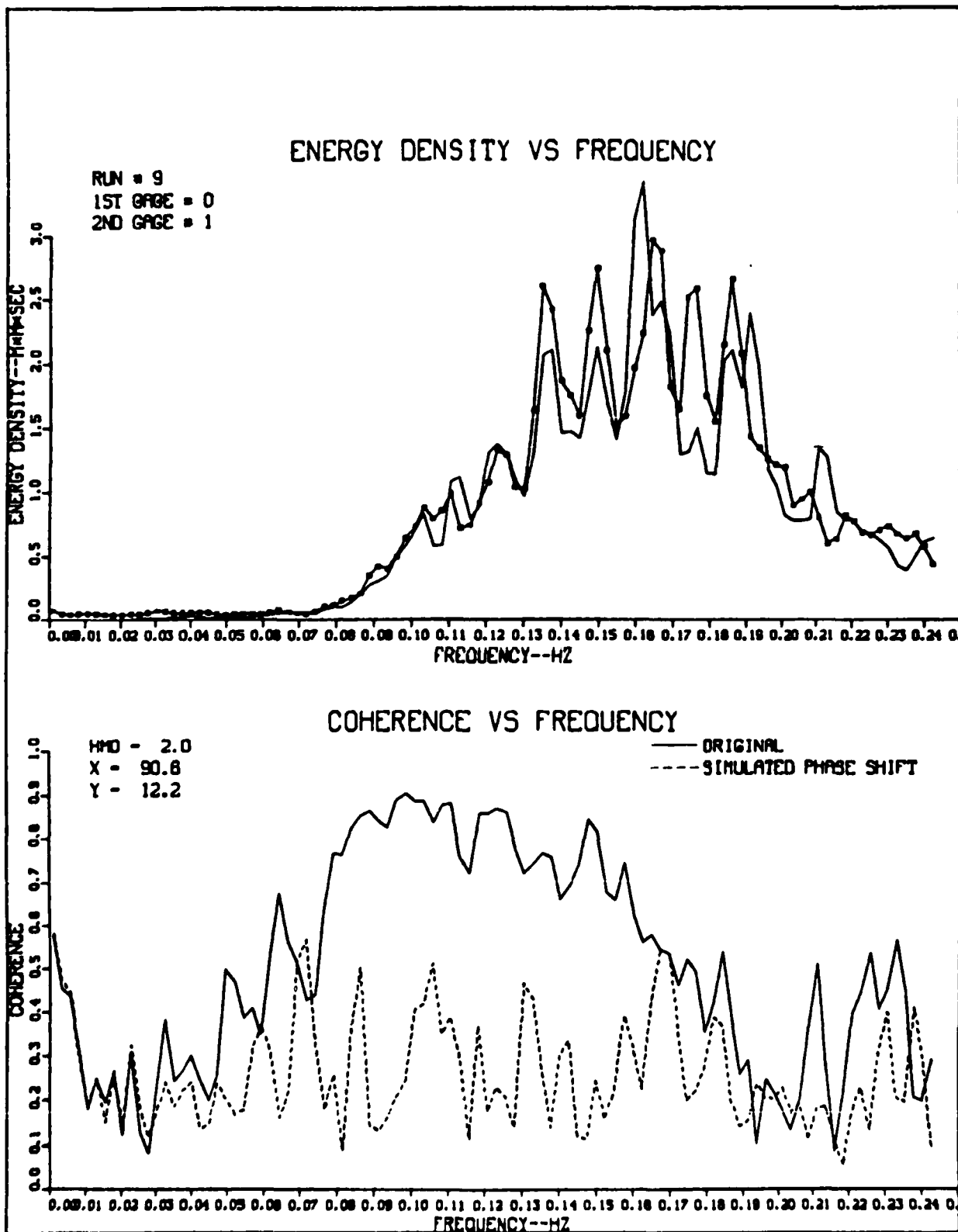


Figure 13. Phase shifted coherence, run 9

PART V: SUMMARY AND RECOMMENDATIONS

31. The primary objective of this experiment was to measure the spatial variability in the wave field under a variety of wave conditions so that findings could assist future ship mooring testing by the NCEL. This report has detailed the experiment and the results obtained directly from the measurements and those obtained through manipulation of the data set. Reference is made to the entire set of plots in Appendix A. The results are presented in terms of the wave coherence function.

32. Qualitatively, the coherence function appears relatively independent of the shape of the spectrum, the spectral energy content, and the location of the spectral peak frequency for the range of conditions examined. The finite water depth at the site appears to render the lower frequency waves less dispersive and, hence, more coherent so long as sufficient energy is present at those frequencies.

33. The most apparent influence on the coherence is the spatial separation, particularly in the along-crest direction. While too much scatter is present to properly quantify the effect of separation, an upper limit is given. It is also possible to construct a set of nondimensionalized coherence contours for the purpose of estimating the coherence function in shallow water. The contours provide a fair estimate in the region of good coherence when compared with actual records, but they overestimate the coherence as the frequency increases beyond about 0.13 Hz.

34. The experiment provided some insight into the variability of the nearshore wave field, and from this knowledge it is possible to make some operational recommendations to the NCEL with regard to their future experiments.

35. The contours developed in Part IV will be helpful in planning ship mooring experiments, but it is evident that the NCEL should also plan to collect onsite data to determine wave coherence. The results indicate that wave coherence rapidly decreases as spatial separation increases, particularly in the along-crest direction.

36. As suggested by the NCEL project engineer, a good experimental procedure would be to place one Waverider buoy a distance d_1 from the ship and a second buoy a distance of d_1 from the first buoy. These buoys should be in line with the ship and oriented directly "up-crest" from the vessel. In this manner wave coherence will be maximized since the along-crest separation

is minimal, and the coherence function found between the two gages can be assumed to be reasonably close to the coherence between the waves at the buoy nearest to the ship and those causing the ship's motion.

37. A certain amount of variation in incoming wave direction can be tolerated without significantly reducing wave coherence, but it will probably be necessary to realign the Waveriders several times over the course of an experiment as wave direction changes. The contours in Figure 9 can be used to estimate allowable limits of wave approach angle variation before the buoys should be moved. To aid in the Waverider relocation, it may be advisable to have an array of vacant buoy mooring installed at the onset of the experiment. Since the mooring array spacings and orientation would have already been determined, the relocation of buoys could proceed more smoothly, particularly in rougher weather. The mooring array configuration can be optimized by the determination of "typical" seasonal wave directions for the particular site.

38. It is highly advisable that the NCEL have at least one backup Waverider gage moored at the site to insure a relative continuity in the data collection. The ideal situation would be to have two backup gages moored in the array in such a fashion as to become the primary gages when the waves approach perpendicularly to the gages' alignment.

39. There is no clear difference in wave coherence between conditions representing swell and storm seas in the data analyzed. Swell waves can be expected to be longer crested and less dispersive and thus less sensitive to spatial separation, but this was not clearly evident in the data. This observation may be a consequence of the finite depth influence, and the difference between sea and swell might become more apparent in deeper water.

40. All of the results were obtained in a water depth of 17 m. Therefore, it is reasonable to expect some signature of the depth in the coherence function. The high coherence values observed in the frequency range 0.08 to 0.1 Hz are quite possibly related to the fact that waves at these frequencies have been rendered less dispersive by the finite depth. Although it is impossible to prove with only the existing data set, it is reasonable to hypothesize that the high coherences at relatively low frequencies are a result of the waves progressing with little alteration in form. According to linear wave theory, the ratio of phase velocity to group velocity for a 0.1-Hz (10-sec) wave in 17-m depth is 1.26. The observed decrease in coherence values at frequencies less than about 0.07 to 0.08 Hz may well be due to the

minuscule amounts of energy at these low frequencies.

41. The data analyzed in this study provide strong evidence of higher coherences at frequencies less than about 0.125 Hz (8-sec period) than at higher frequencies. This trend appears unrelated to the form of the autospectrum. Since one intention of mooring experiments is to have high coherence at energy-containing frequencies affecting ship motion, wave fields with energy primarily at frequencies lower than 0.125 Hz should be preferred for the experiment.

42. The mooring lines for the Waveriders should have the same scope to minimize the variation in buoy separation distance. The wave-induced buoy displacements are not thought to be a factor in the large fluctuations in the coherence function. This is supported by Kuo, Mitsuyasu, and Masuda (1979a, 1979b) in which the same coherence fluctuations appear between wave gages which have been rigidly fixed in position. Change in separation distance between the moored ship and the nearest Waverider will depend on the freedom of movement in the ship's mooring system and the ship's dynamic response to the mooring line forces.

43. Sea states having multiple wavetrains approaching from different directions exhibit wave coherence functions which deteriorate more rapidly than sea states with single wavetrains and a single central direction. When recording multiple wavetrains, it is best to align with the direction containing the most energy. However, the presence of multiple wavetrains will certainly complicate data analysis and interpretation.

44. The following recommendations are offered with regard to future NCEL ship mooring experiments.

- a. Align the two Waverider buoys parallel with the central incident wave direction.
- b. Place additional Waverider moorings in the array to facilitate buoy relocation.
- c. Relocate Waveriders when feasible to maintain the desired alignment with the wave field.
- d. Maintain equal scope on all the wave gage moorings.
- e. Moor at least one (more if possible) backup Waverider at the experiment site.

- f. If a choice exists, avoid collecting experimental data during wave conditions with energy concentrated at the higher frequencies (greater than 0.13 Hz) and during sea states with multiple wavetrains approaching from different directions.

REFERENCES

- Briggs, M. J. 1981 (Aug). "Multichannel Maximum Entropy Method of Spectral Analysis Applied to Offshore Structures," WHOI-81-69, Woods Hole Oceanographic Institution, Woods Hole, Mass.
- Kuo, Y., Mitsuyasu, H., and Masuda, A. 1979a (Jul). "Experimental Study on the Phase Velocity of Wind Waves, Part 1: Laboratory Wind Waves," Reports of Research Institute for Applied Mechanics, Vol XXVII, No. 83.
- _____. 1979b (Sep). "Experimental Study on the Phase Velocity of Wind Waves, Part 2: Ocean Waves," Reports of Research Institute for Applied Mechanics, Vol XXVII, No. 84.
- Mattie, M. G., and Harris, D. L. 1979 (Sep). "A System for Using Radar to Record Wave Direction," TR 79-1, US Army Coastal Engineering Research Center, Ft. Belvoir, Va.
- Thompson, E. F. 1982 (Aug). "Nonrandom Behavior in Field Wave Spectra and Its Effect on Grouping of High Waves," TR 82-2, US Army Coastal Engineering Research Center, Ft. Belvoir, Va.

Table 1

Data Collection

Data Collection Run Number	Date	Start Time	Analysis		Data Collection		Start Time	Analysis Run Number
			Run Number	Number	Run Number	Number		
1	23 April	1300	1	21	25 April	1300	5	
2	23 April	1900	2	22	3 May	0700	5	
3	23 April	2120	2	23	6 May	1102	5	
4	23 April	2240	2	24	9 May	0900	5	
5	23 April	2400	2	25	17 May	0115	6	
6	24 April	0300	3	26	17 May	0905	6	
7	24 April	0420	3	27	17 May	1200	7	
8	24 April	0540	3	28	17 May	1700	7	
9	24 April	0700	4	29	17 May	1820	7	
10	24 April	0900	4	30	17 May	2100	7	
11	24 April	1020	4	31	17 May	2220	7	
12	24 April	1140	4	32	17 May	2340	7	
13	24 April	1300	4	33	18 May	0040	7	
14	24 April	1700	4	34	18 May	0300	7	
15	24 April	1820	4	35	18 May	0420	7	
16	24 April	2100	4	36	18 May	0719	7	
17	24 April	2220	4	37	19 May	0702	8	
18	24 April	2340	4	38	10 June	0600	9	
19	25 April	0100	4					
20	25 April	0700	4					

Table 2

Analyzed Data Set

Analysis Run No.	H_m^* m	T_p^{**} sec	Wave Direction† deg	Wind Speed m/sec	Wind Direction deg	Data Collection Run No.
1	0.5	8-9	Primary 130 Secondary 55	4	133	1
2	0.8	3.6	125-130	9-11	132-153	2
3	2.5	9-9.5	125	6.7	203	6
4	1.6	9.5	125	7	219-230	9
5	1.1	10.5	Primary 45 Secondary 125	7.5	290	21
6	2.0	7.0	55	12	32	25
7	1.3	6-7	55	7	32	27
8	1.1	5.5	Primary 110 Secondary 80		137-155	37
9	1.9	6.5	80	9.4	34	38

* H_m equals four times the standard deviation of sea surface elevations.

** T_p is the wave period associated with the spectral peak.

† 0° - North, 90° - East, 180° - South, 270° - West.

APPENDIX A: COHERENCE PLOTS

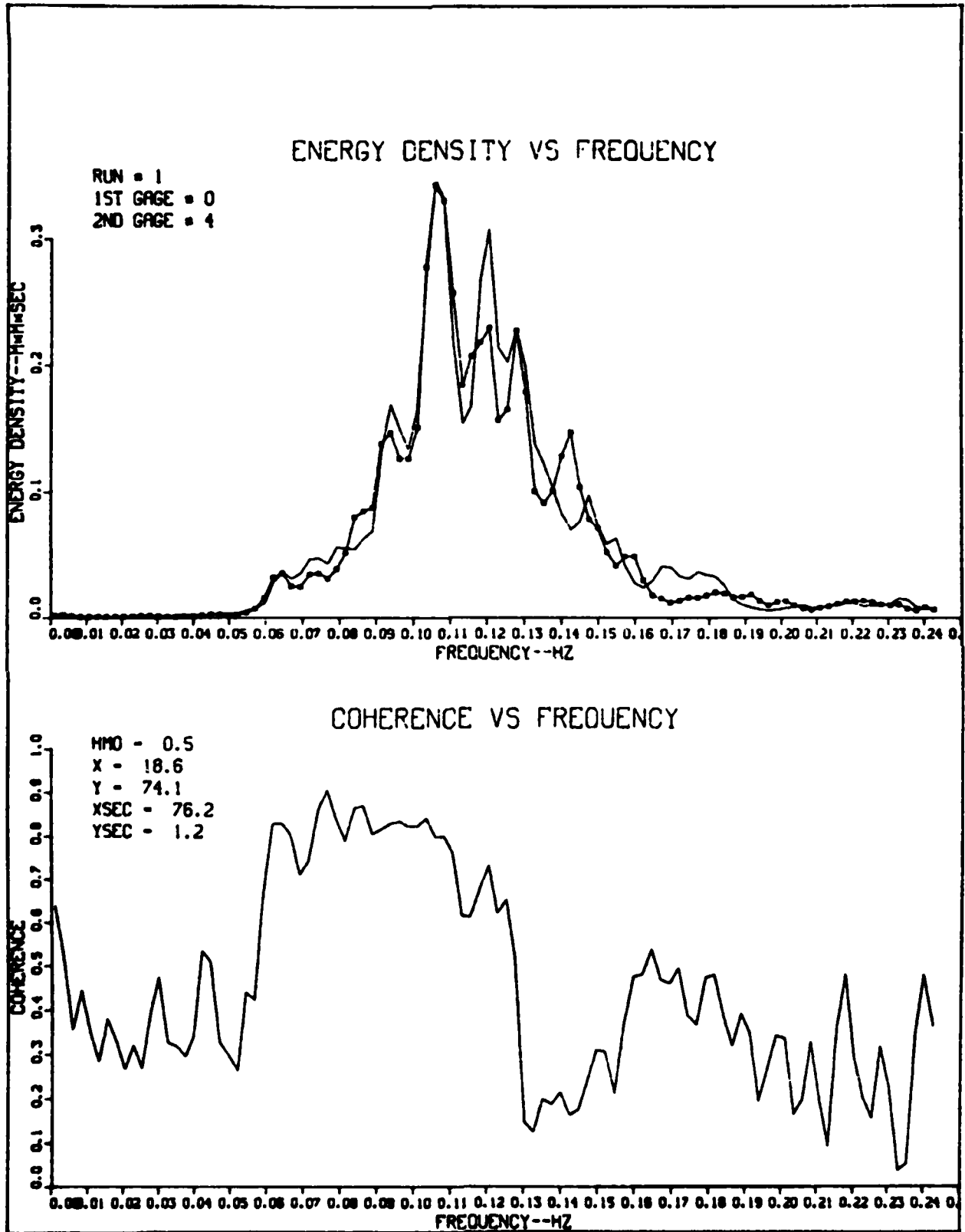


Figure A1. Analysis run 1 of gages 0 and 4

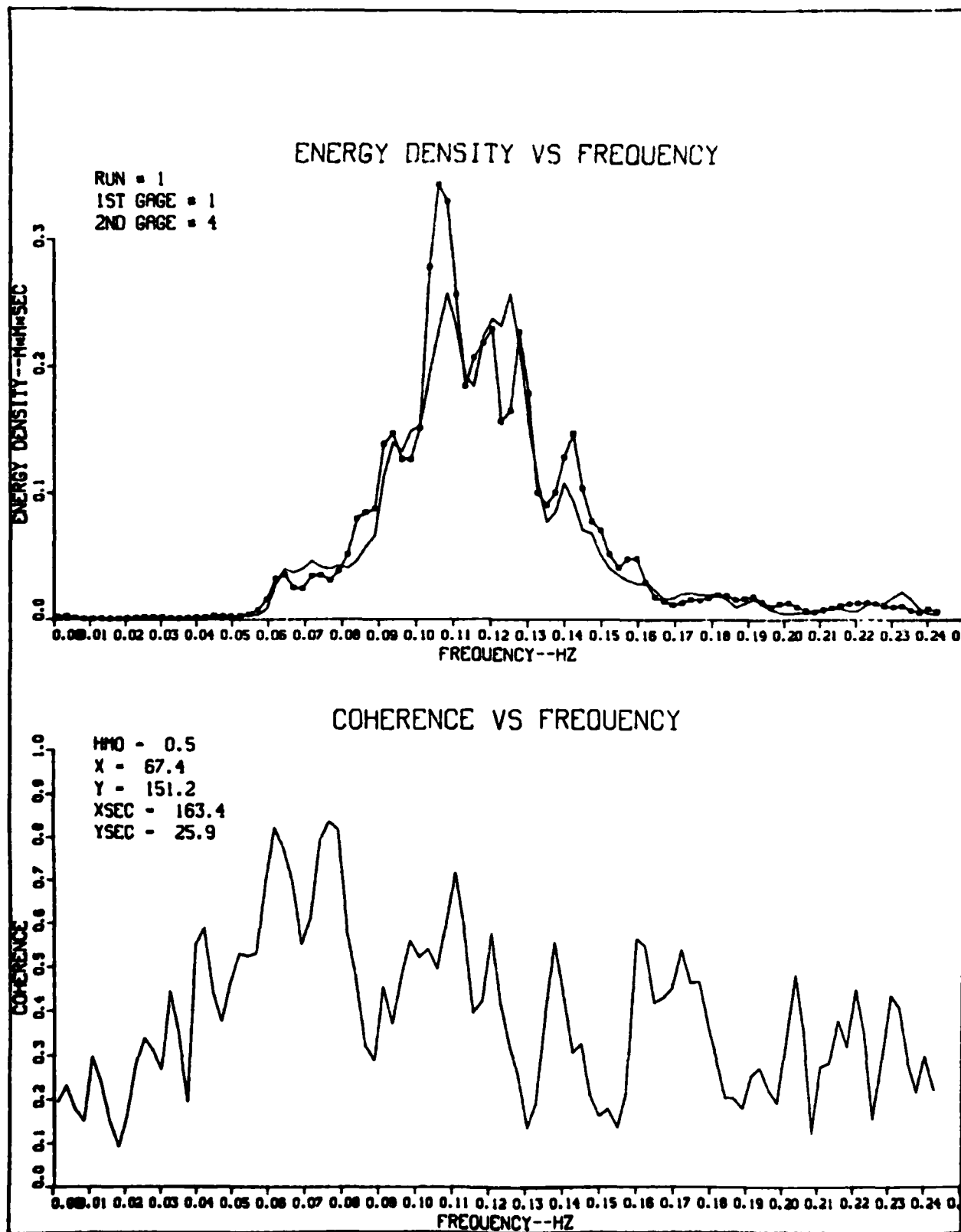


Figure A2. Analysis run 1 of gages 1 and 4

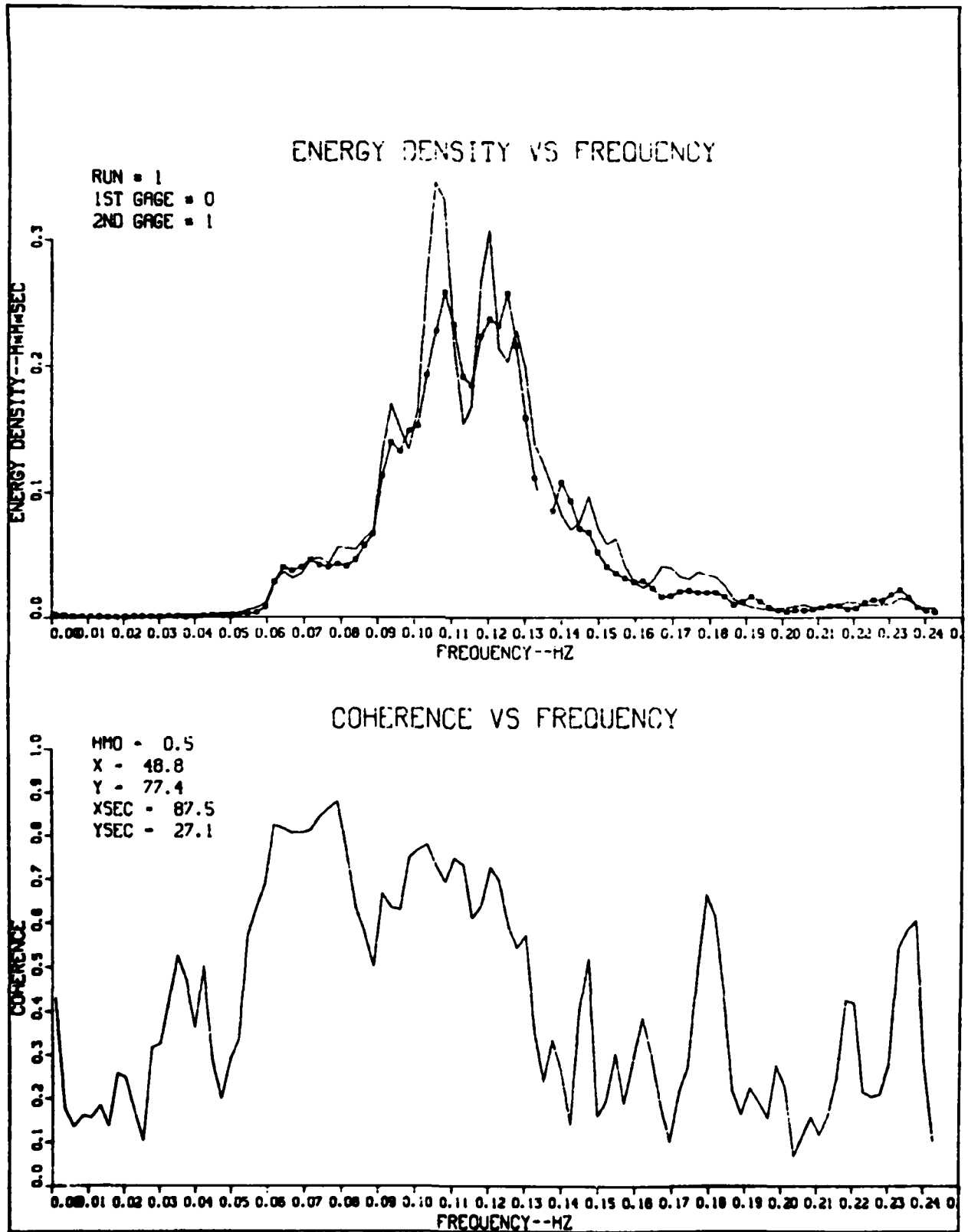


Figure A3. Analysis run 1 of gages 0 and 1

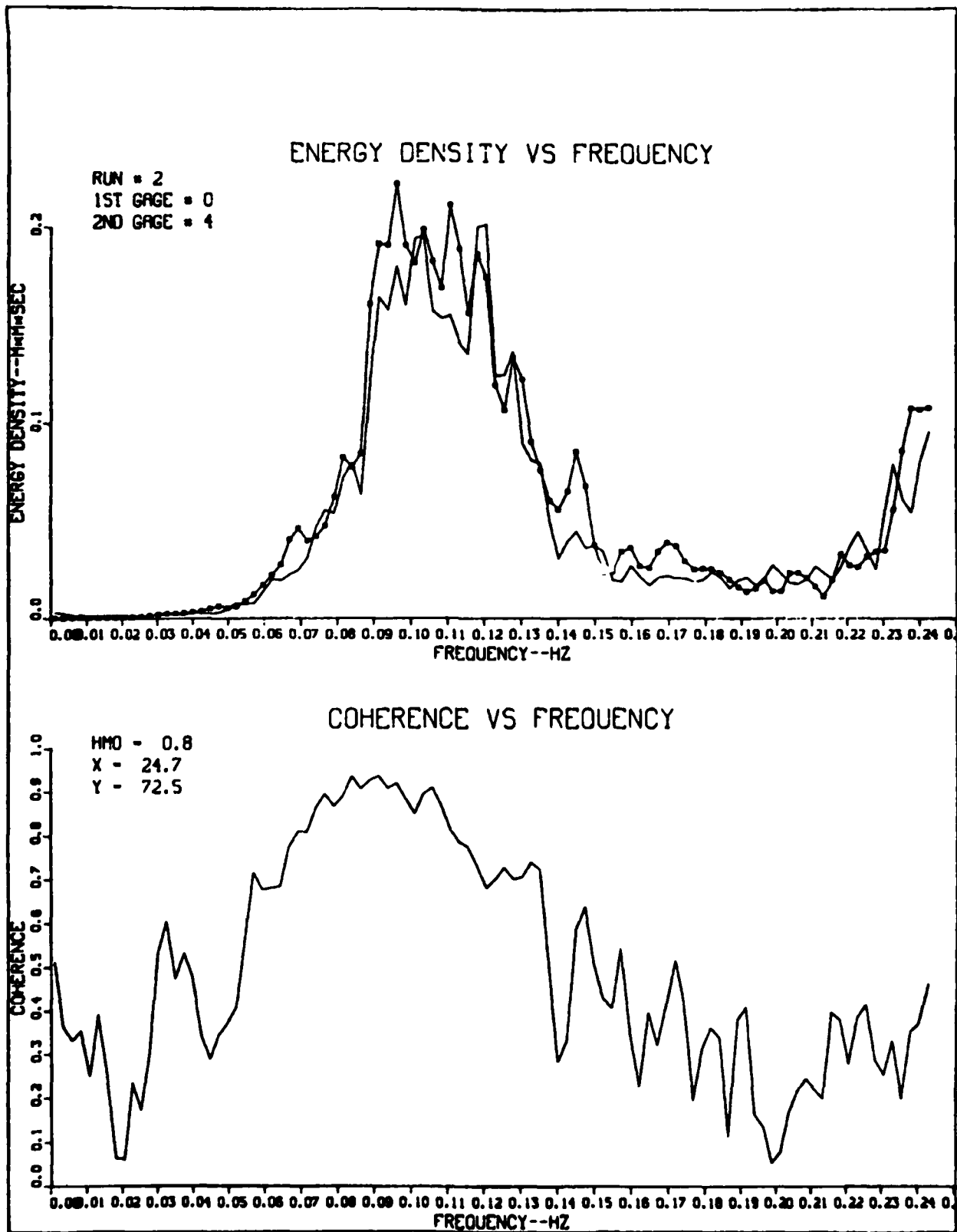


Figure A4. Analysis run 2 of gages 0 and 4

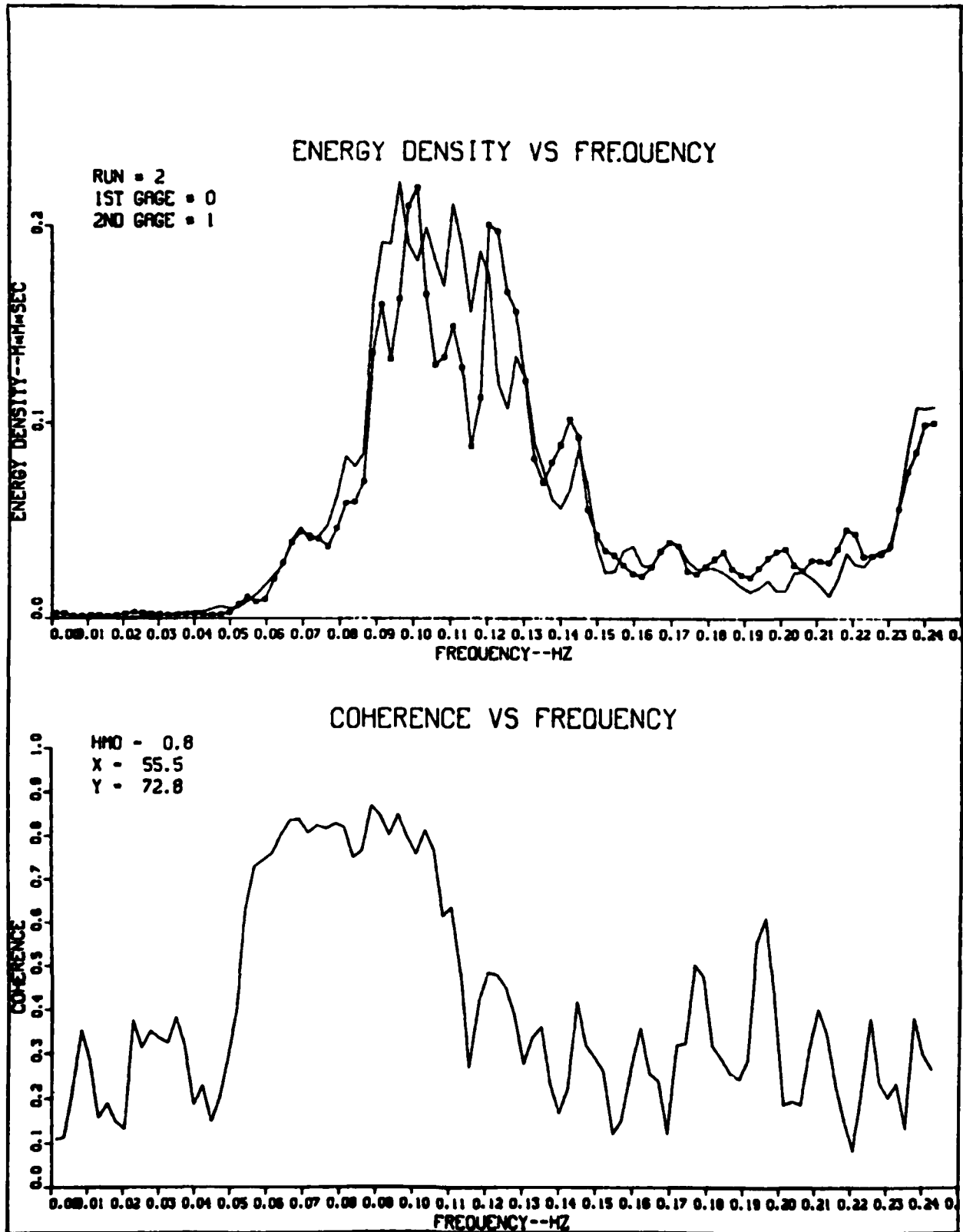


Figure A5. Analysis run 2 of gages 0 and 1

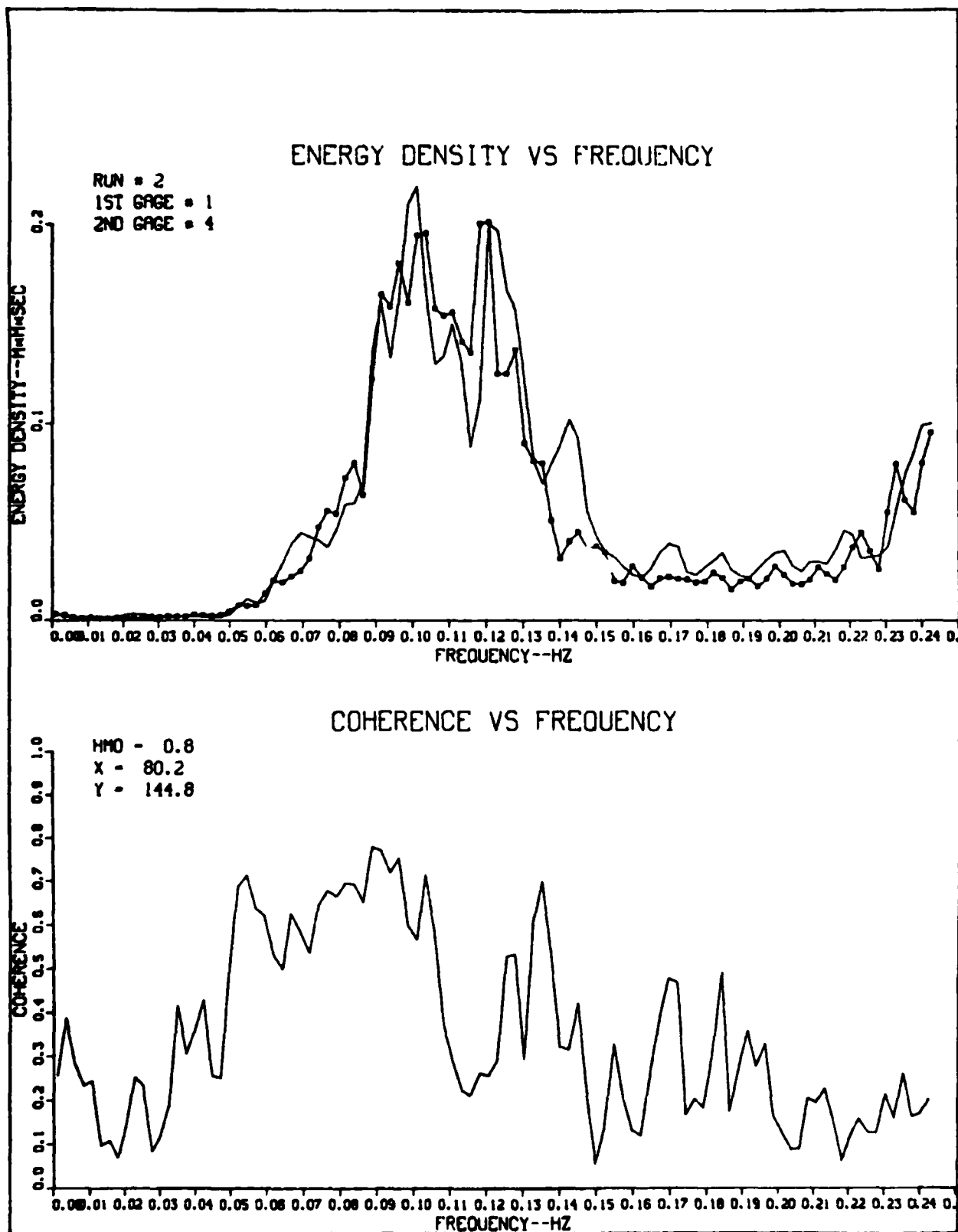


Figure A6. Analysis run 2 of gages 1 and 4

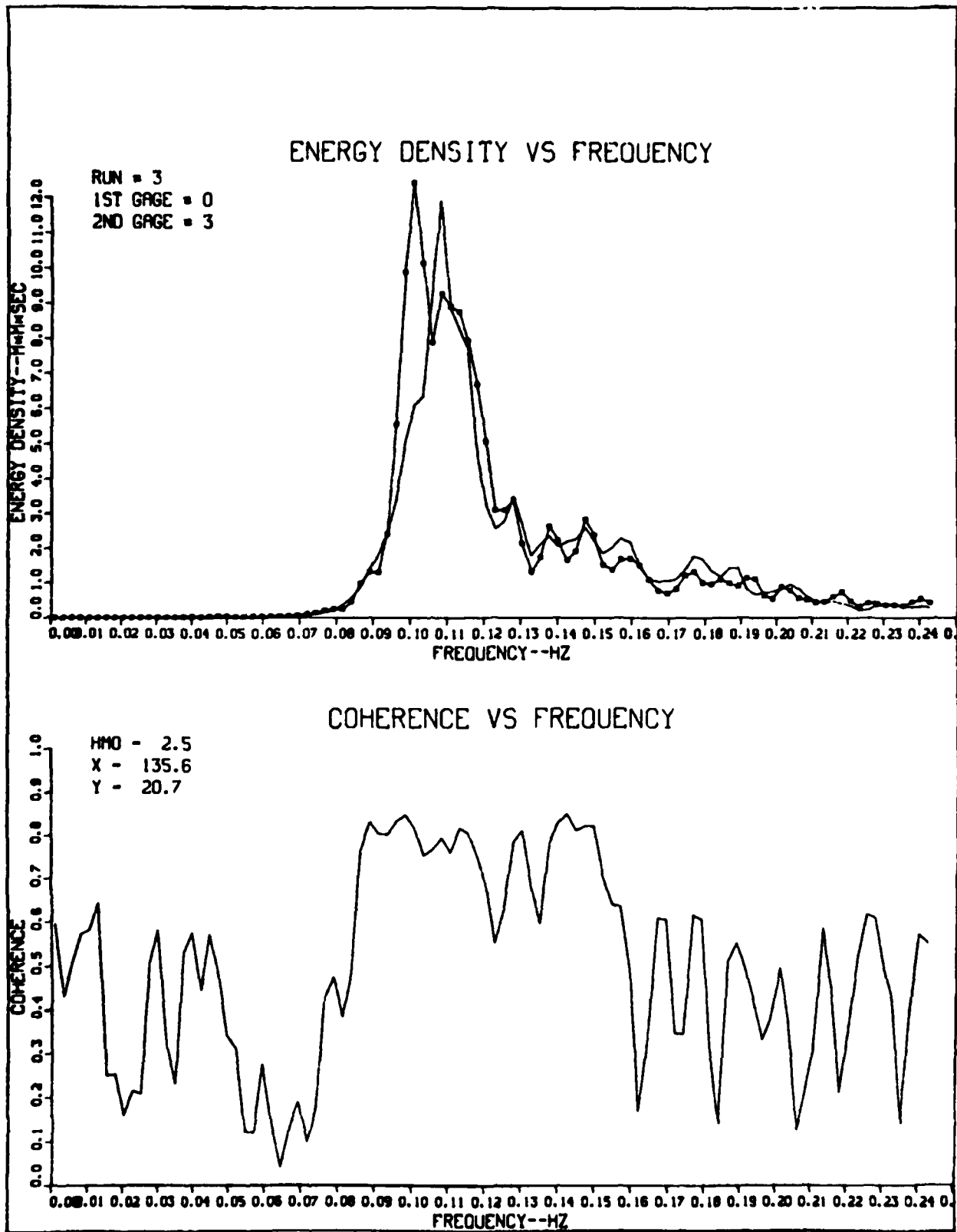


Figure A7. Analysis run 3 of gages 0 and 3

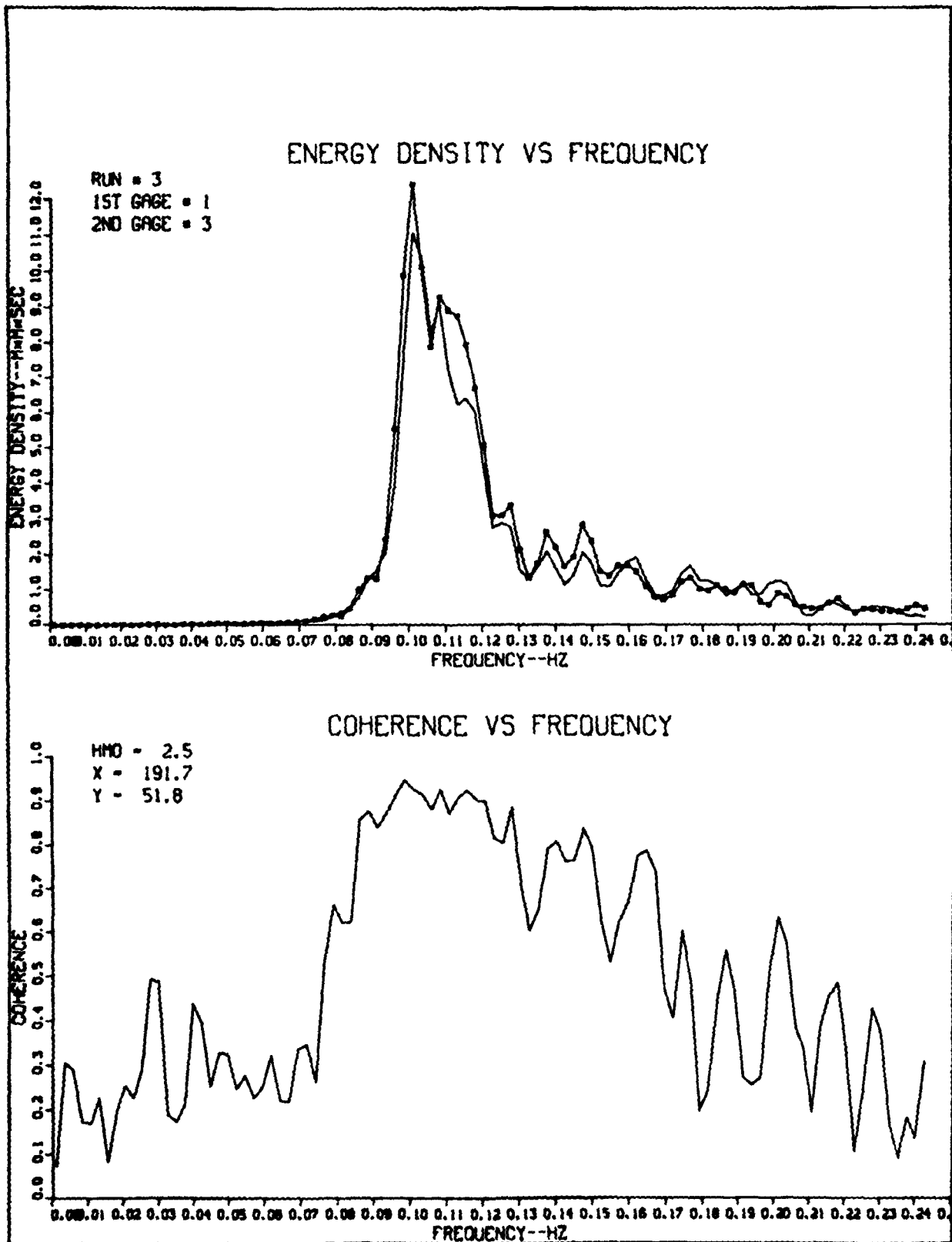


Figure A8. Analysis run 3 of gages 1 and 3

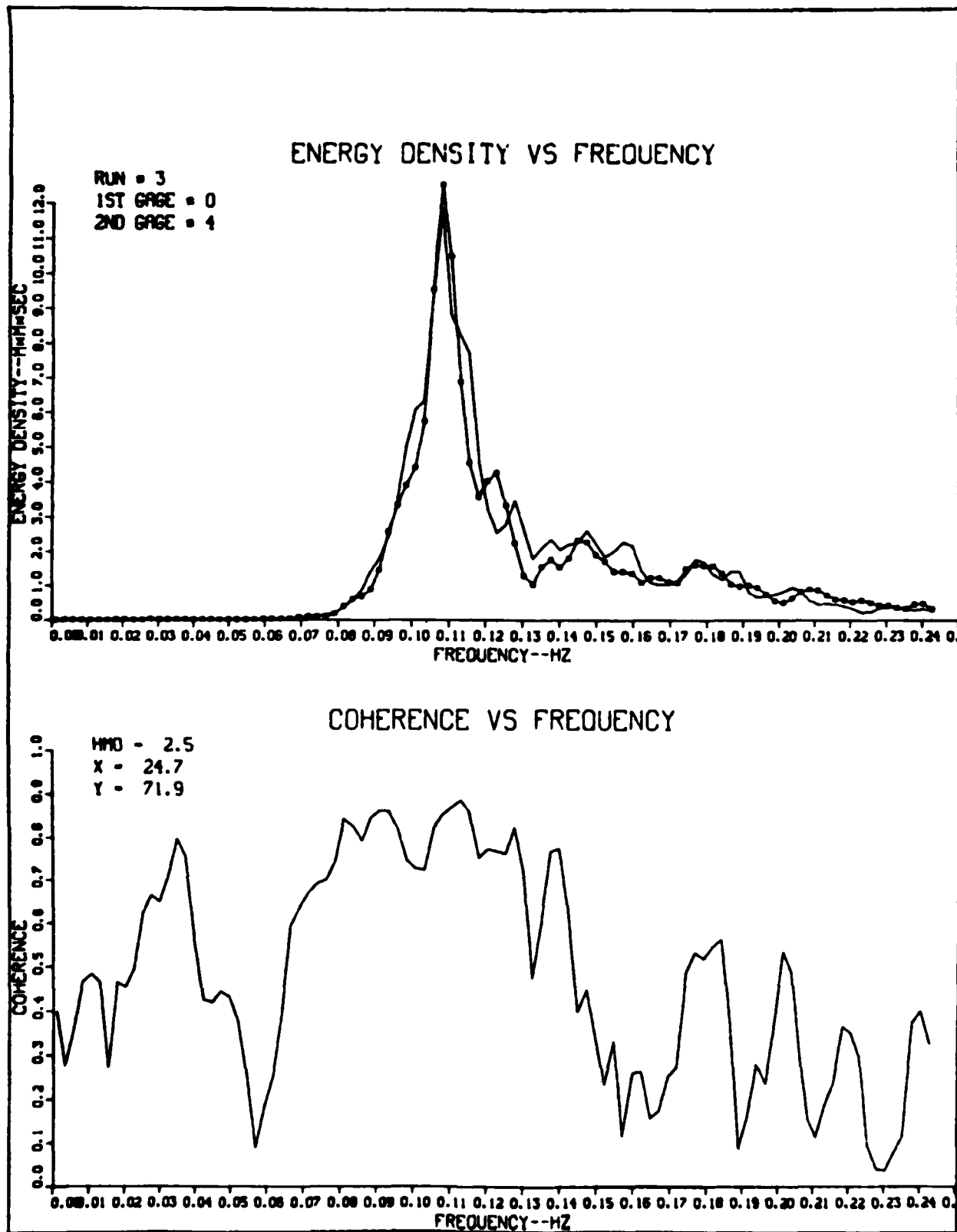


Figure A9. Analysis run 3 of gages 0 and 4

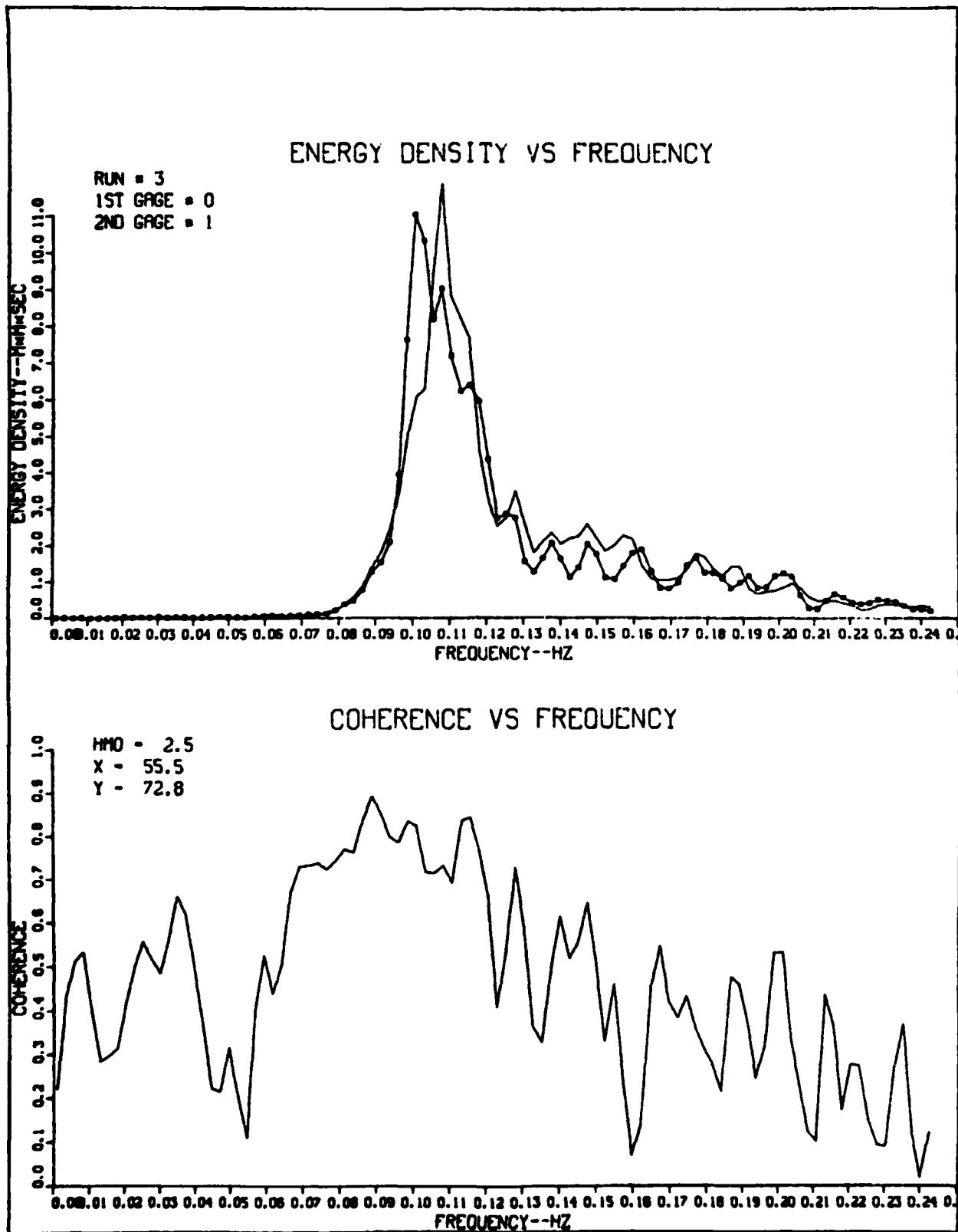


Figure A10. Analysis run 3 of gages 0 and 1

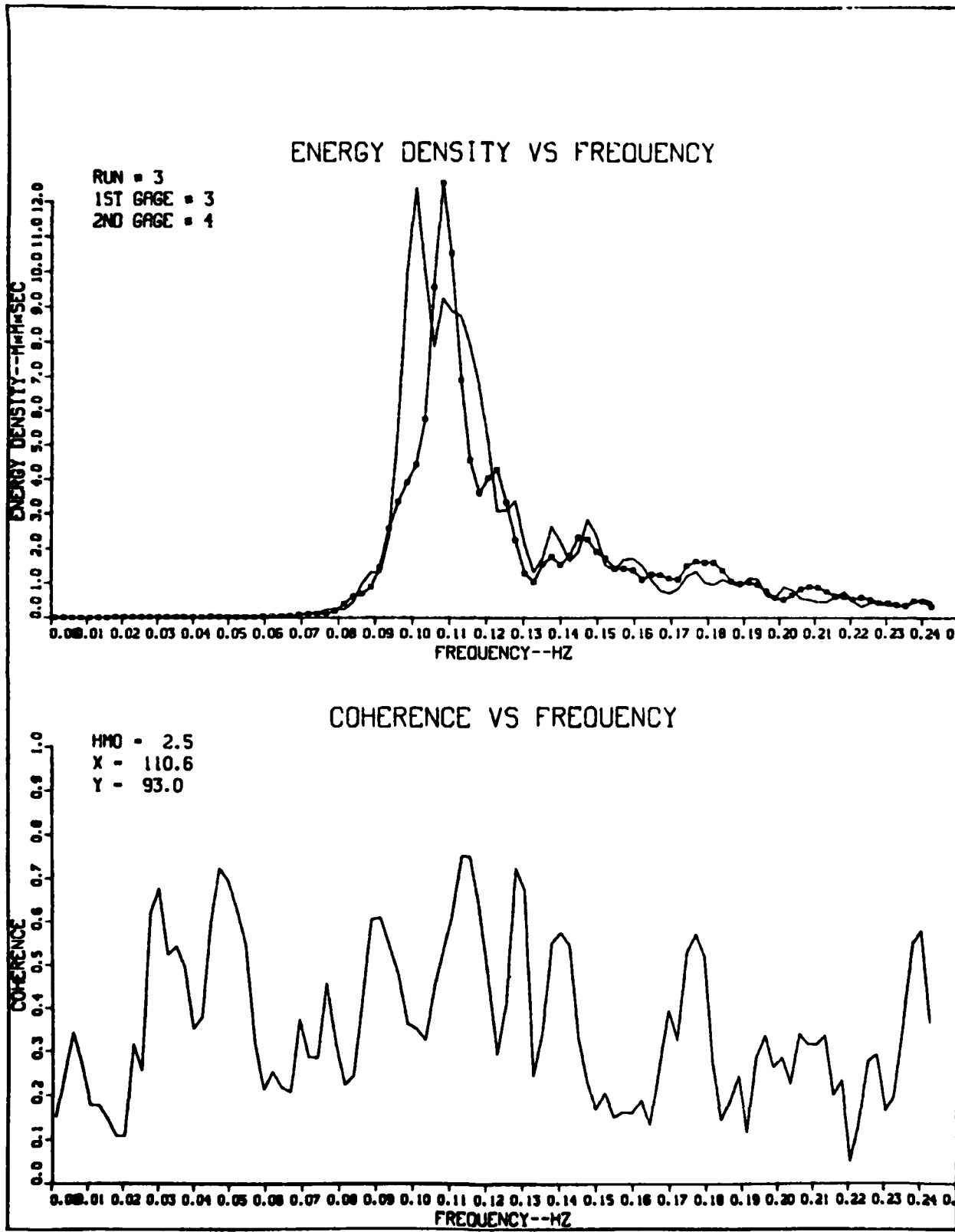


Figure A11. Analysis run 3 of gages 3 and 4

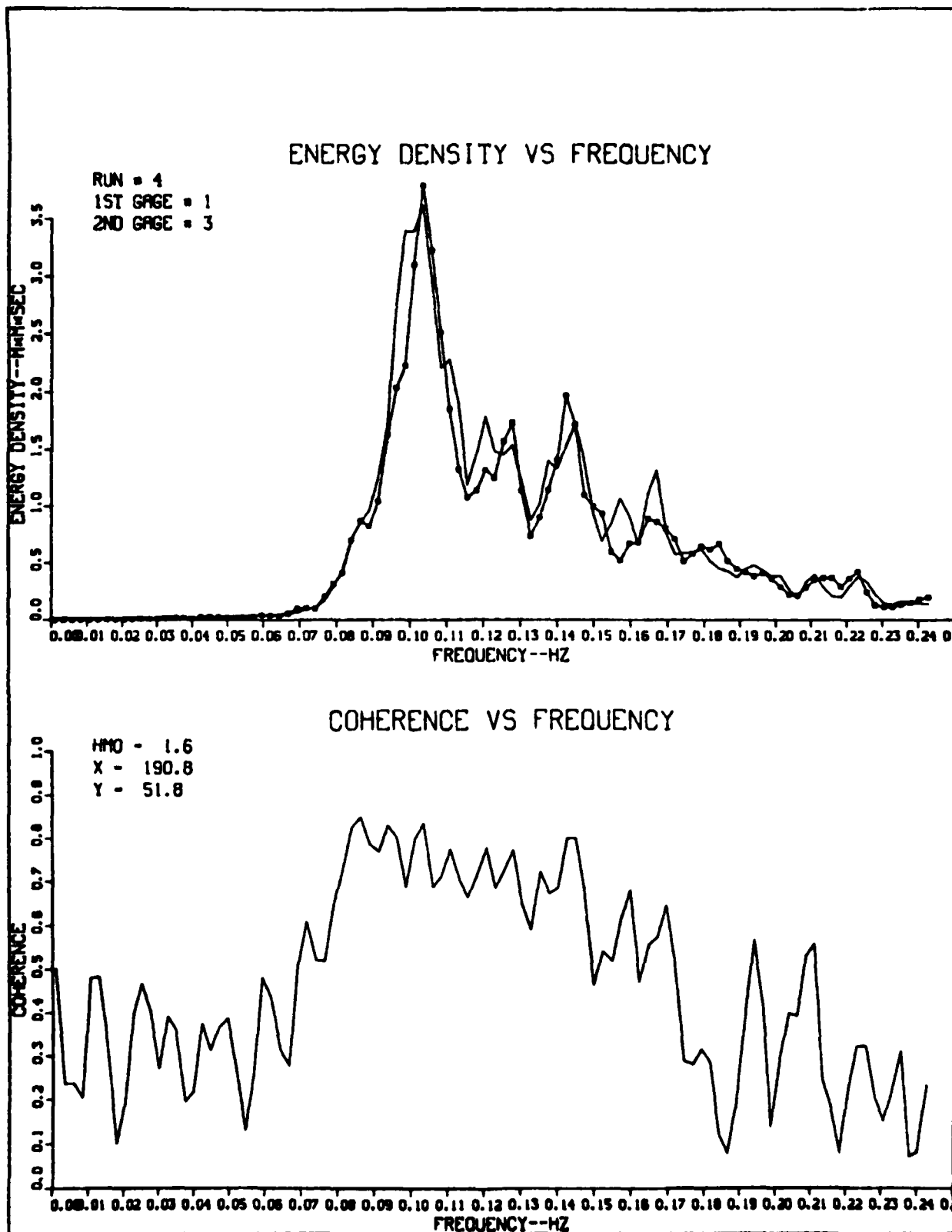


Figure A12. Analysis run 4 of gages 1 and 3

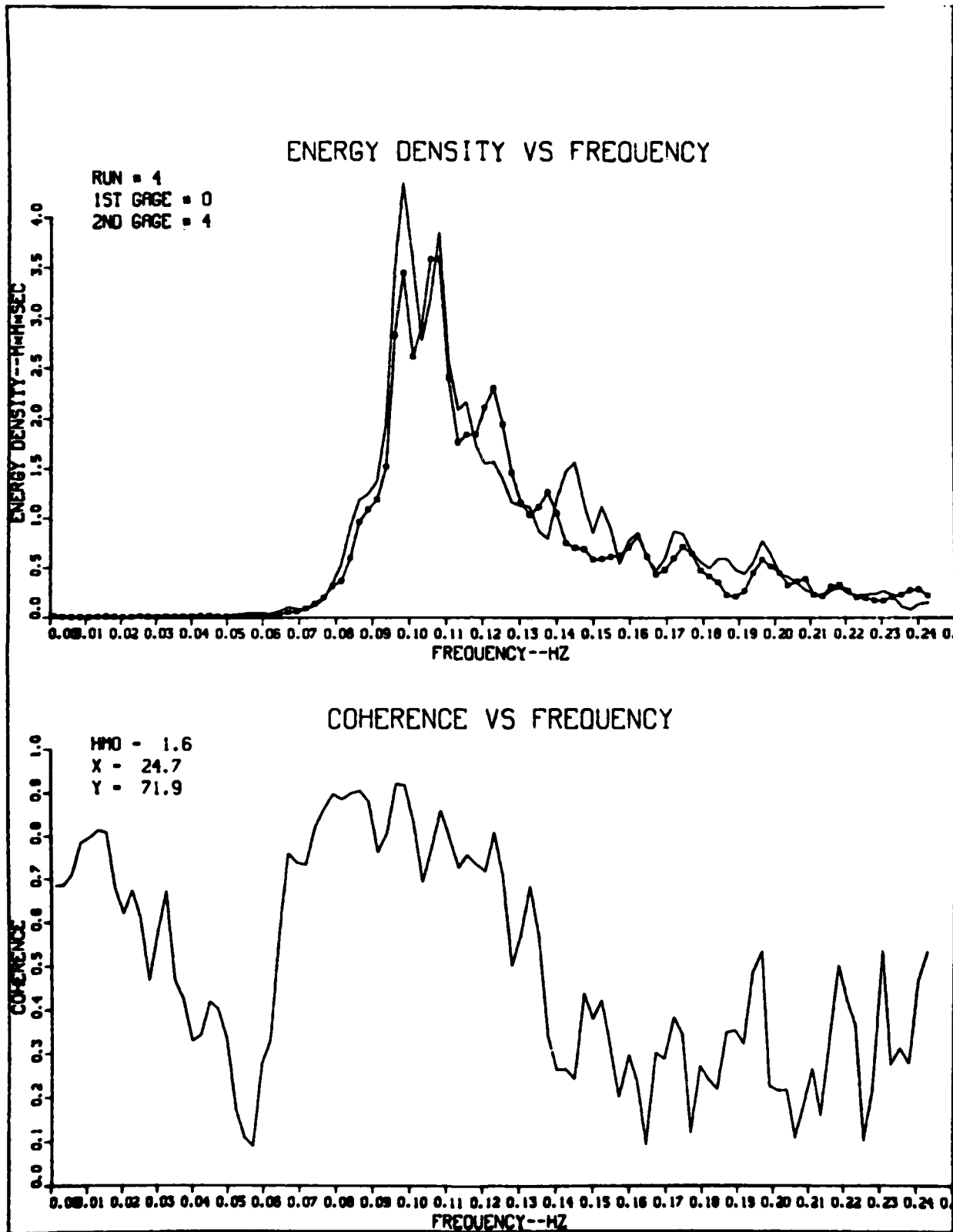


Figure A13. Analysis run 4 of gages 0 and 4

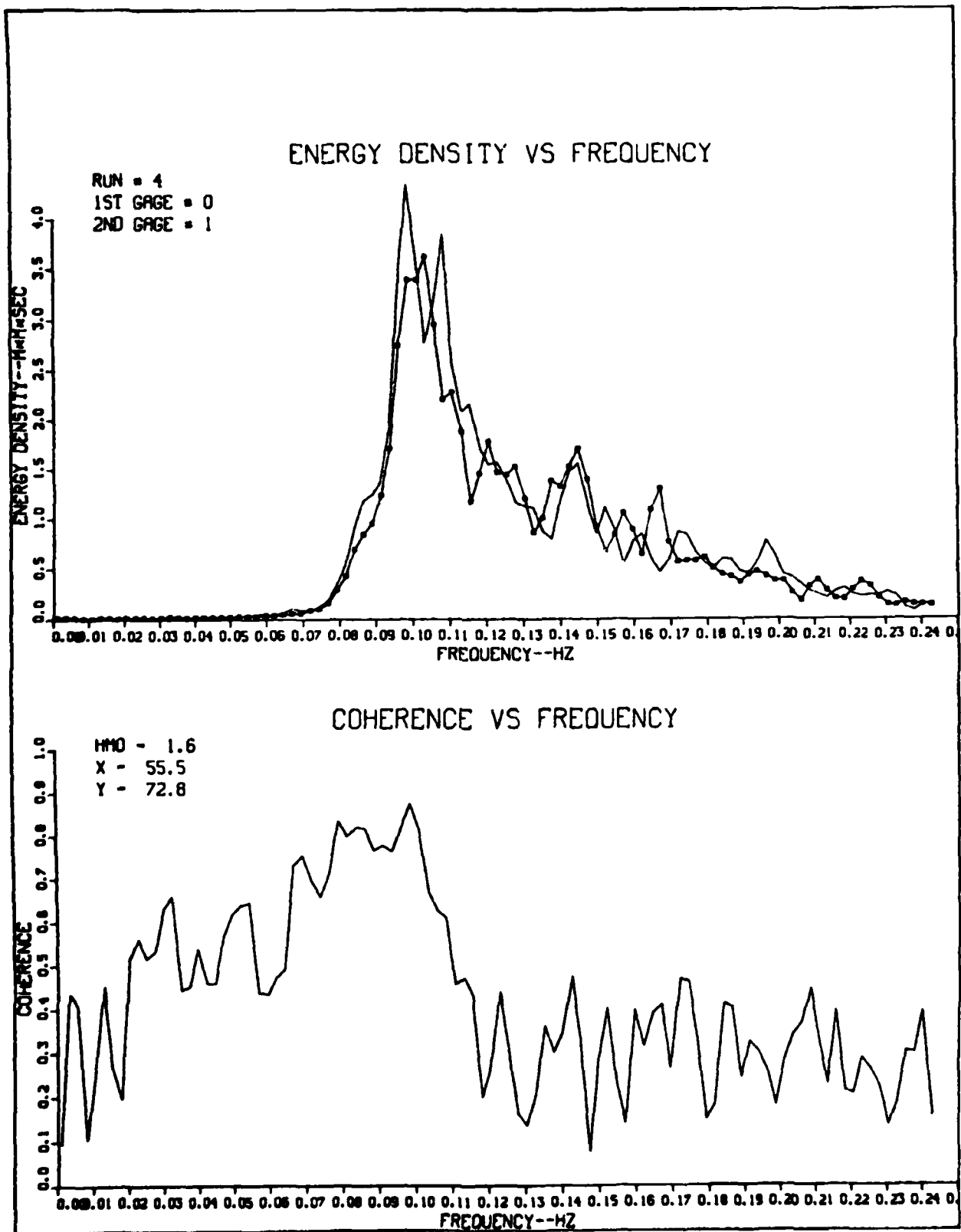


Figure A14. Analysis run 4 of gages 0 and 1

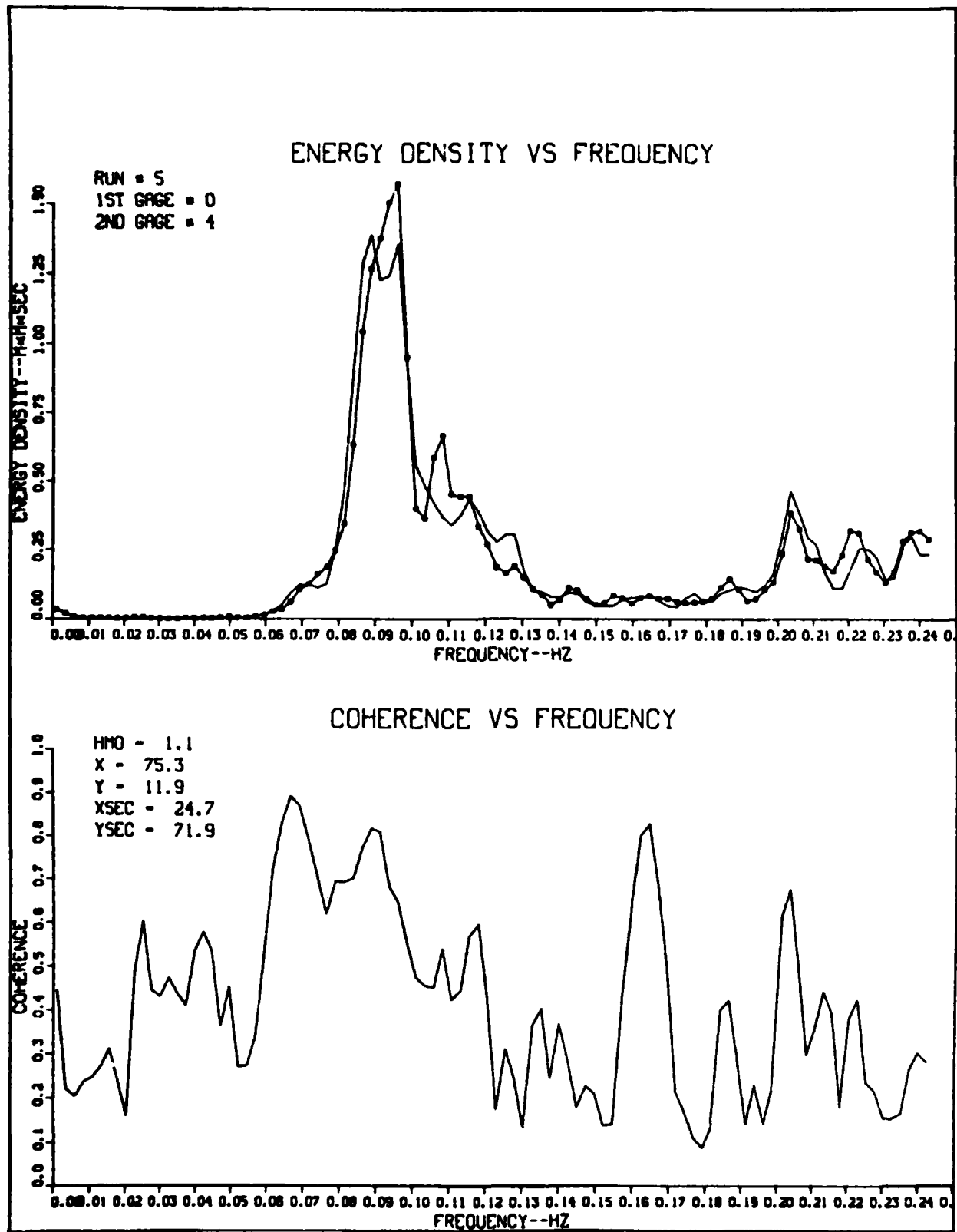


Figure A15. Analysis run 5 of gages 0 and 4

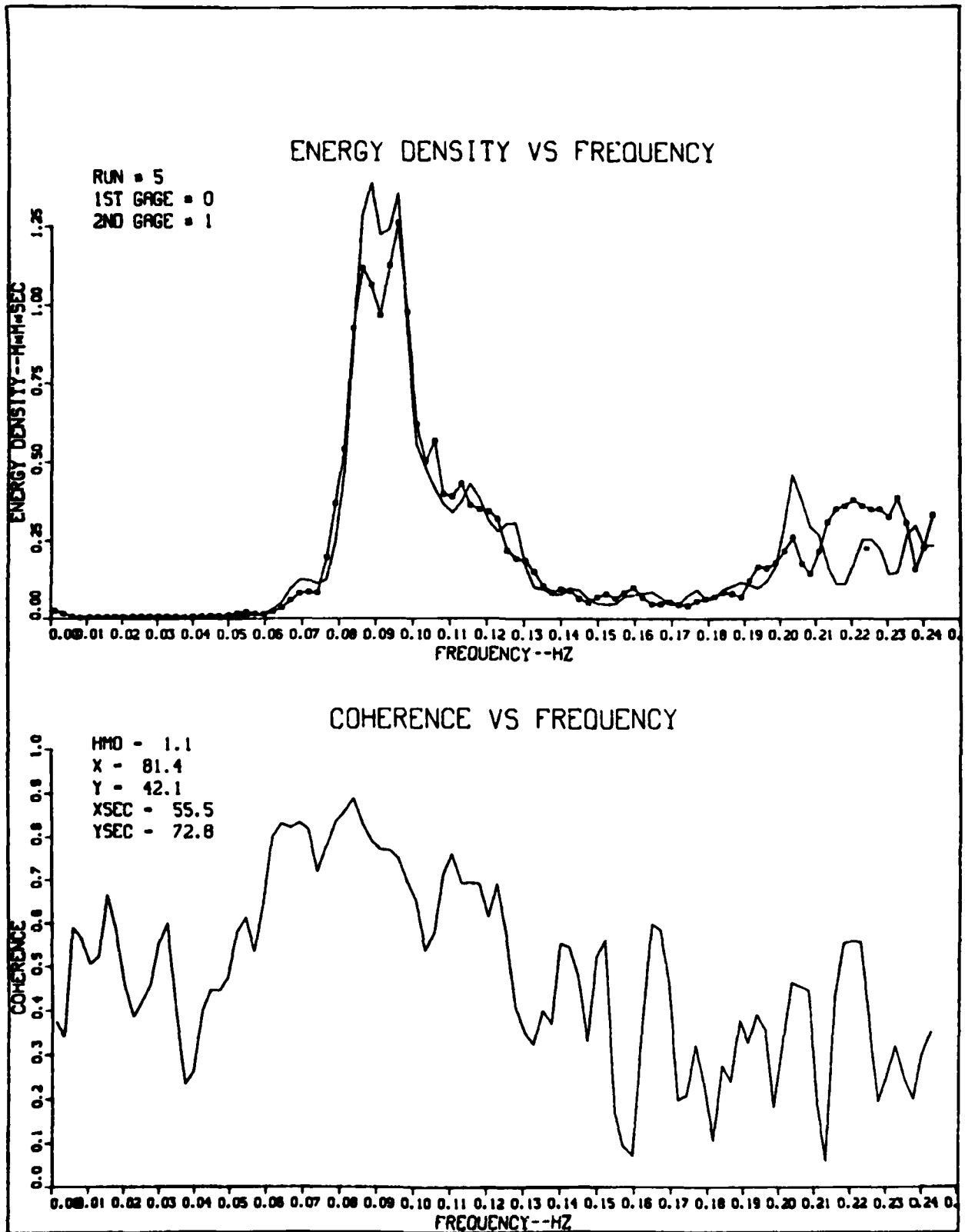


Figure A16. Analysis run 5 of gages 0 and 1

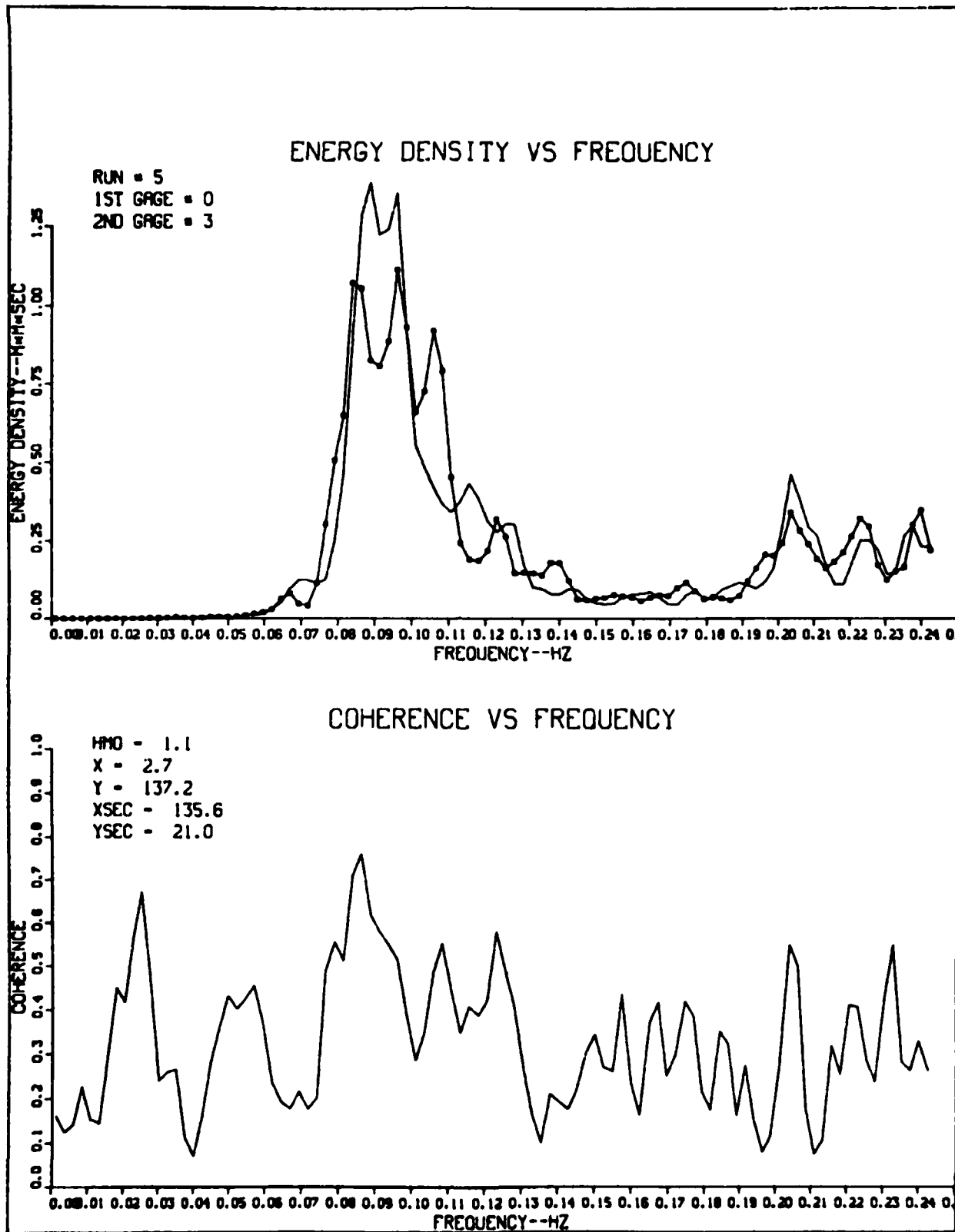


Figure A17. Analysis run 5 of gages 0 and 3

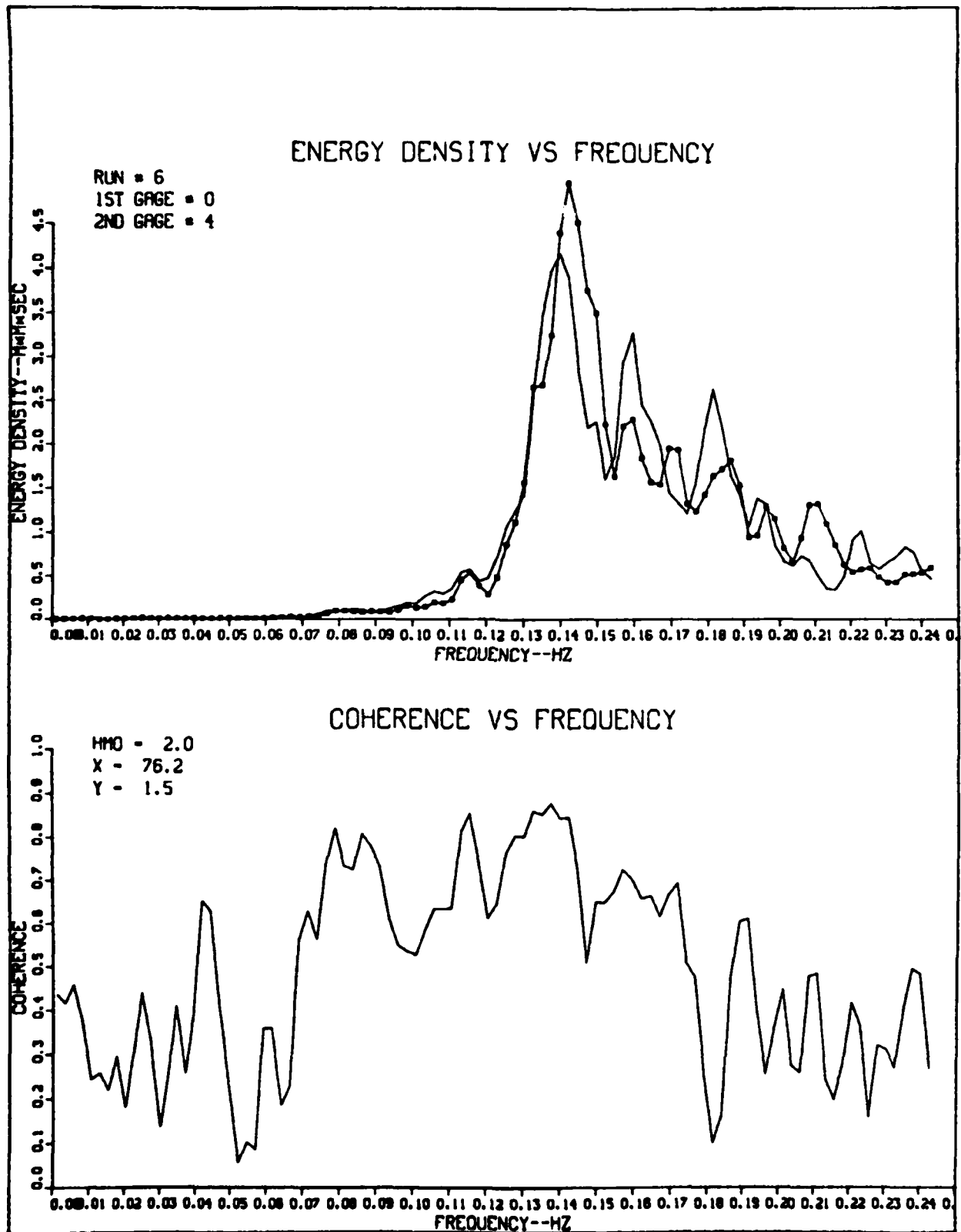


Figure A18. Analysis run 6 of gages 0 and 4

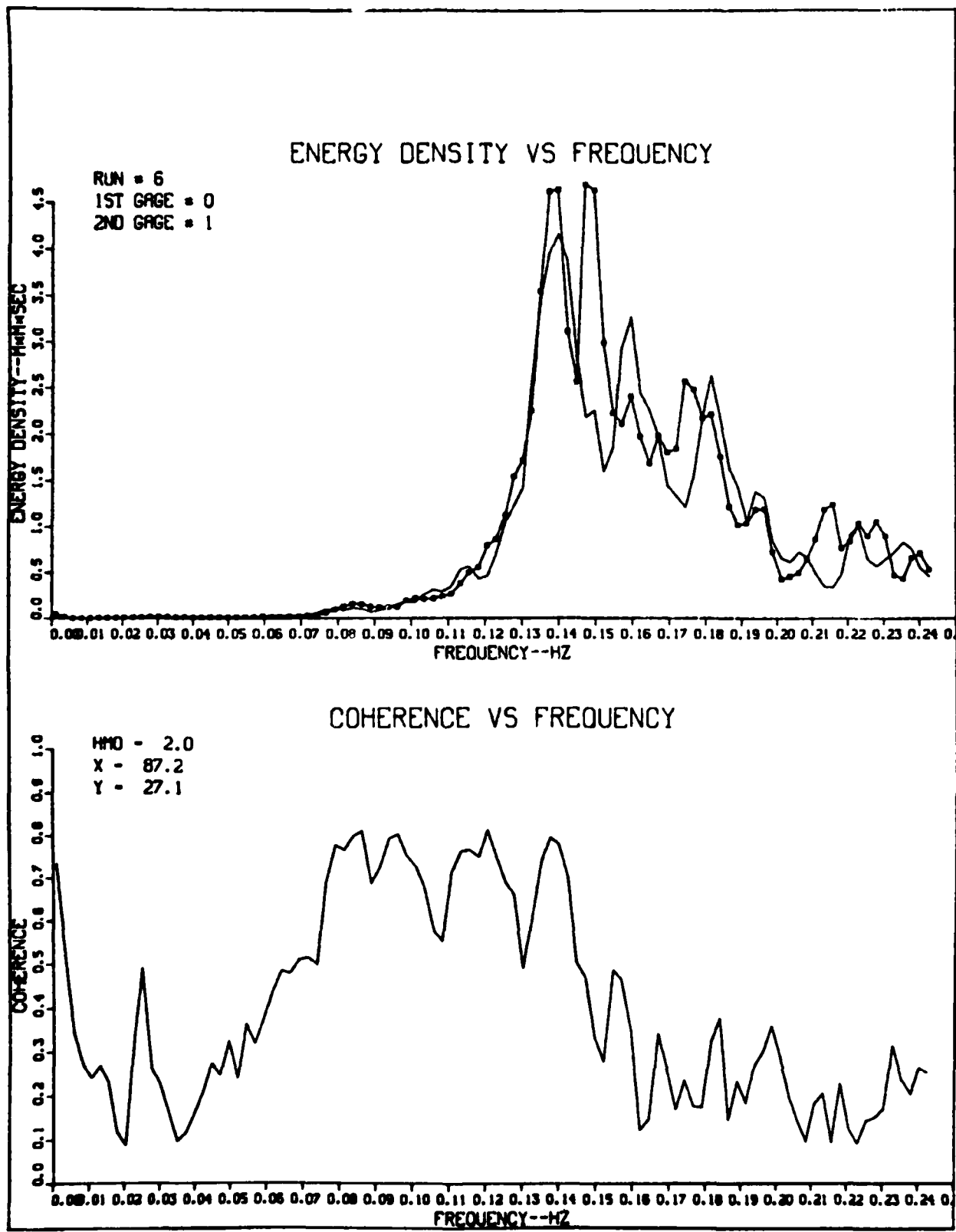


Figure A19. Analysis run 6 of gages 0 and 1

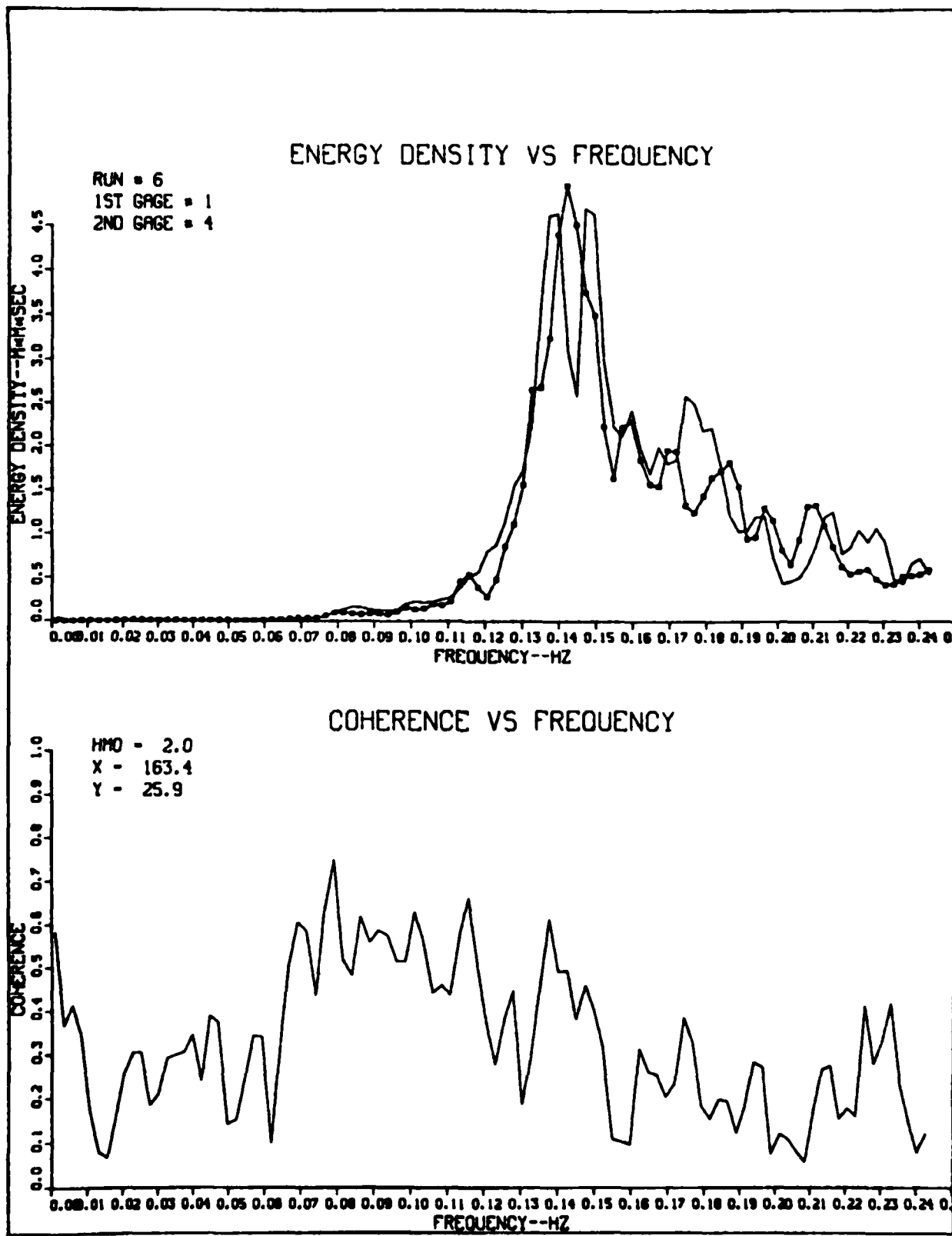


Figure A20. Analysis run 6 of gages 1 and 4

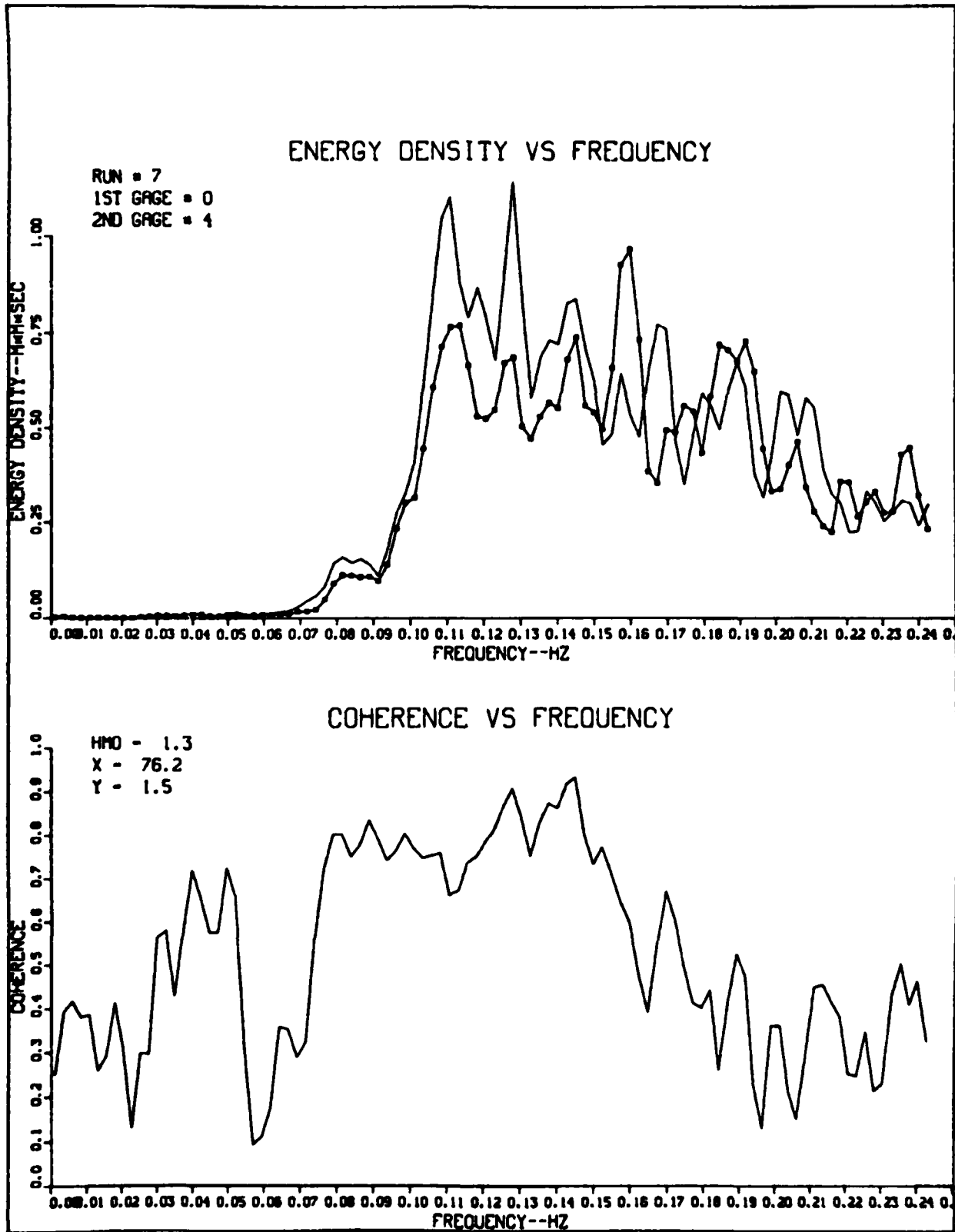


Figure A21. Analysis run 7 of gages 0 and 4

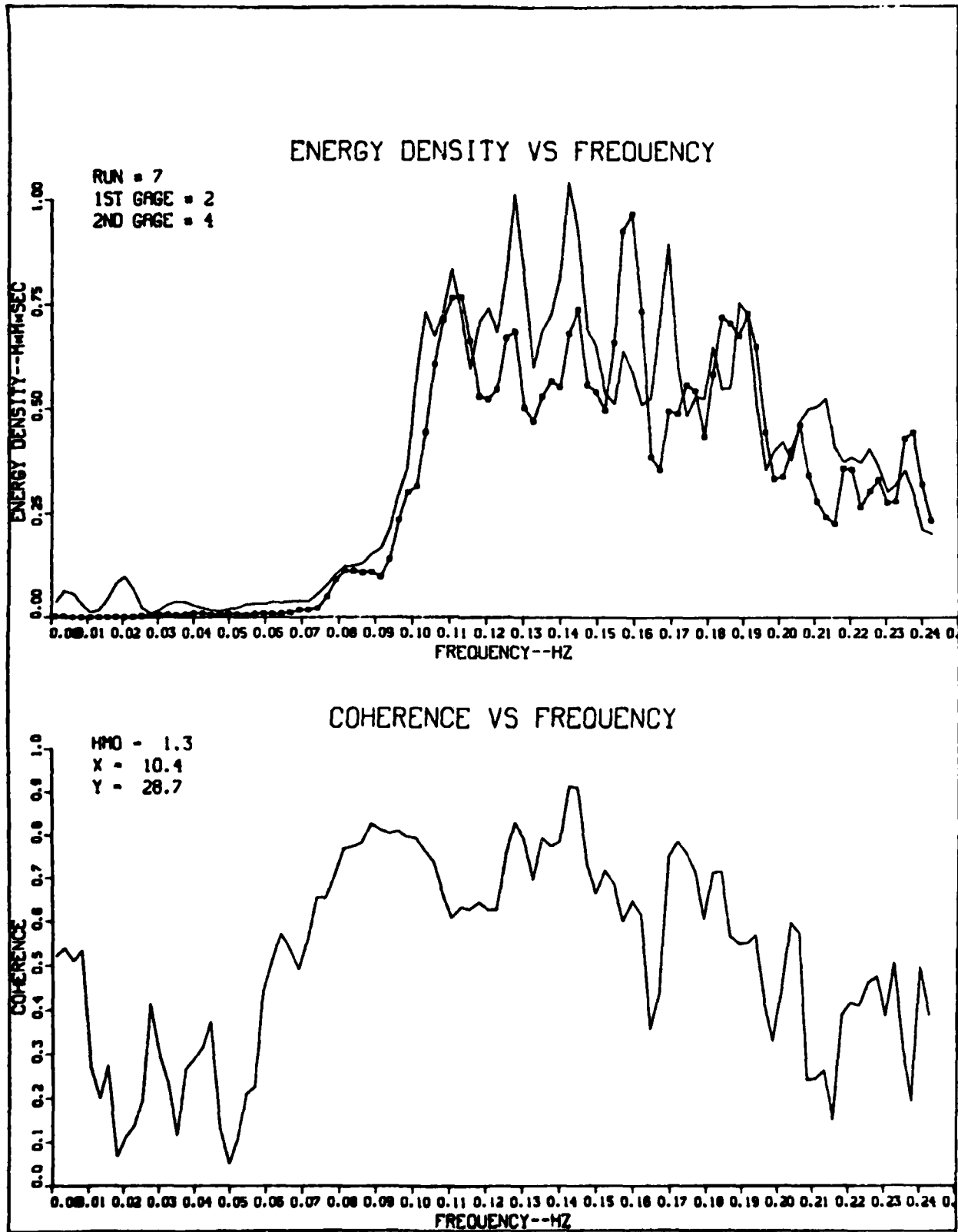


Figure A22. Analysis run 7 of gages 2 and 4

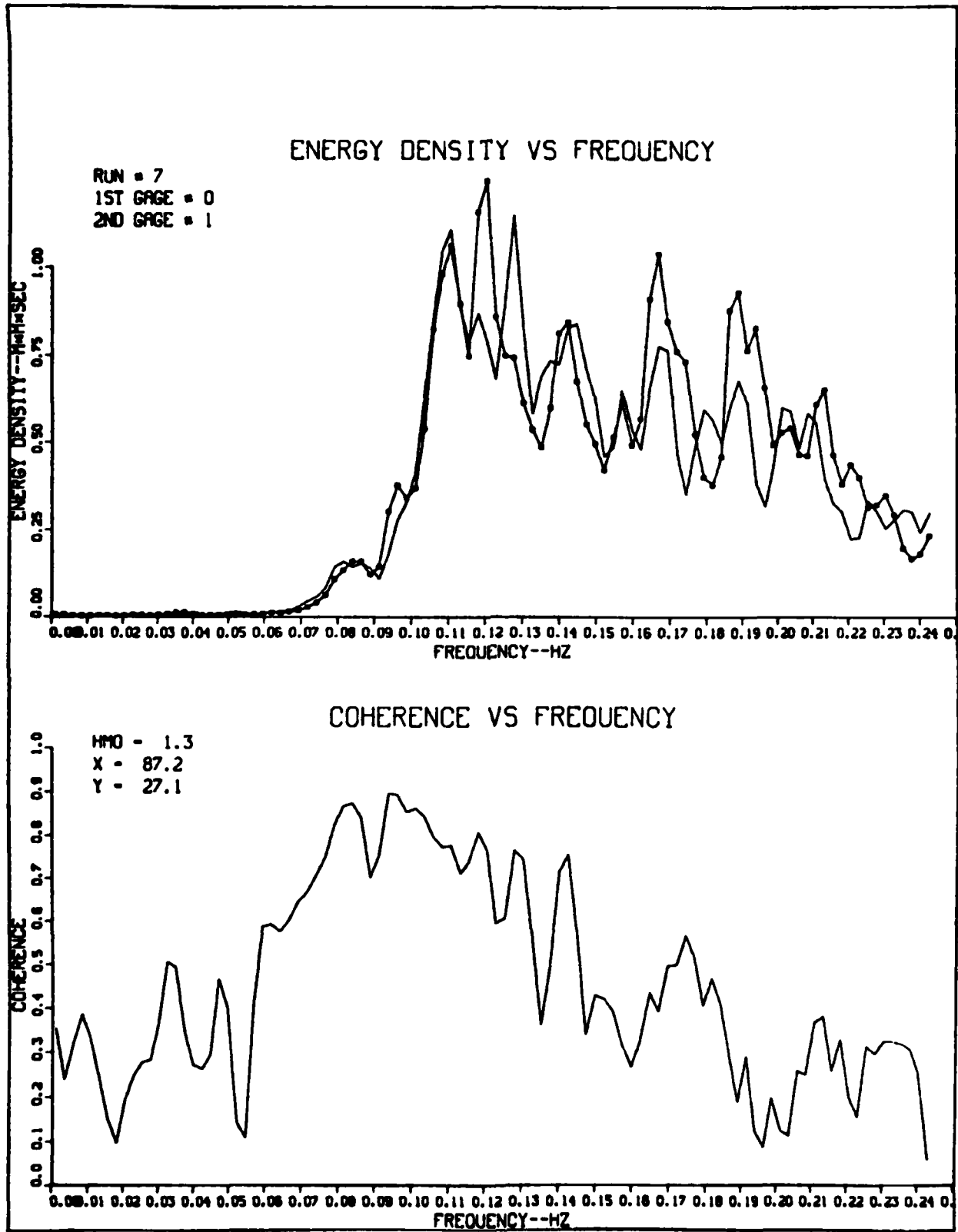


Figure A23. Analysis run 7 of gages 0 and 1

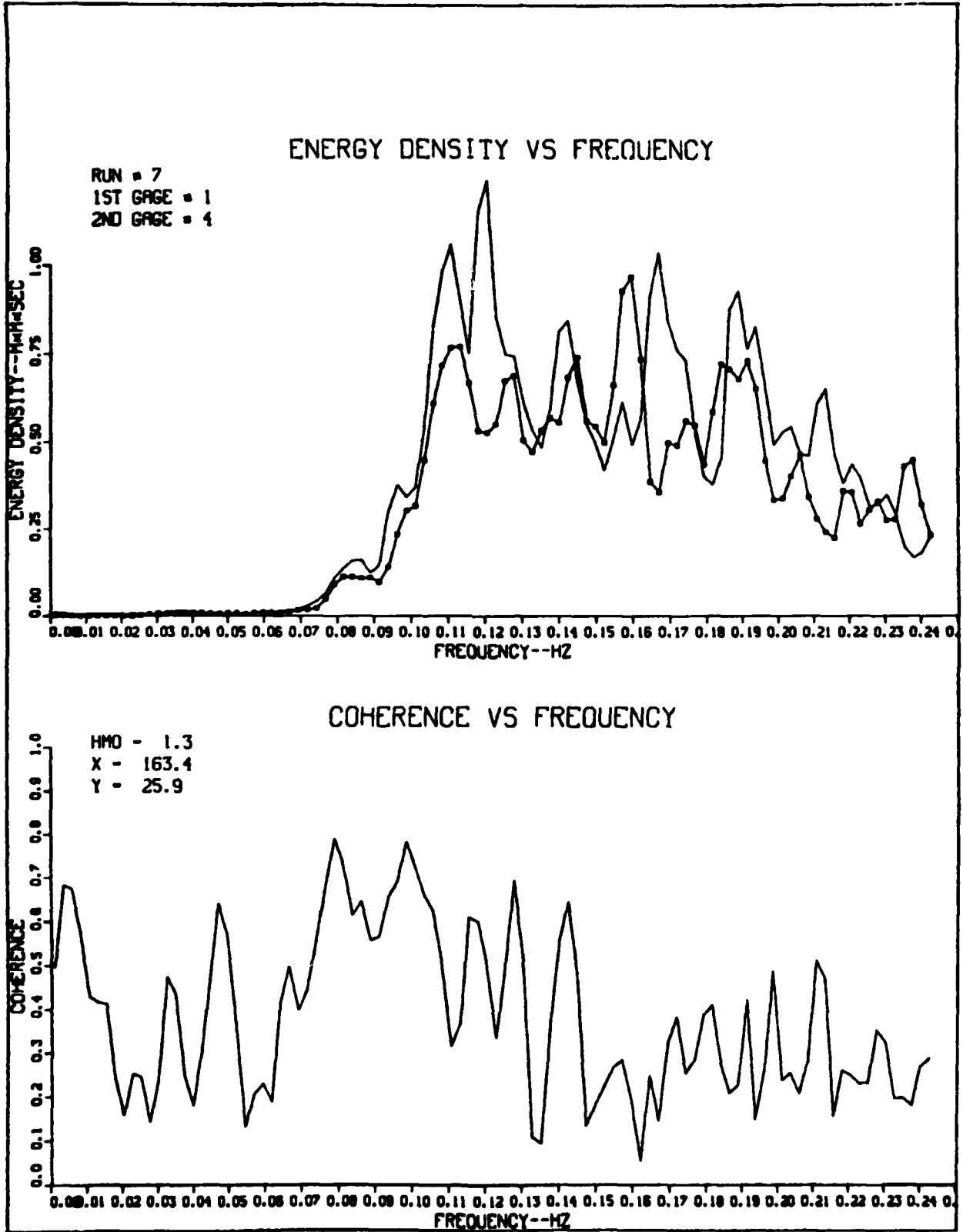


Figure A24. Analysis run 7 of gages 1 and 4

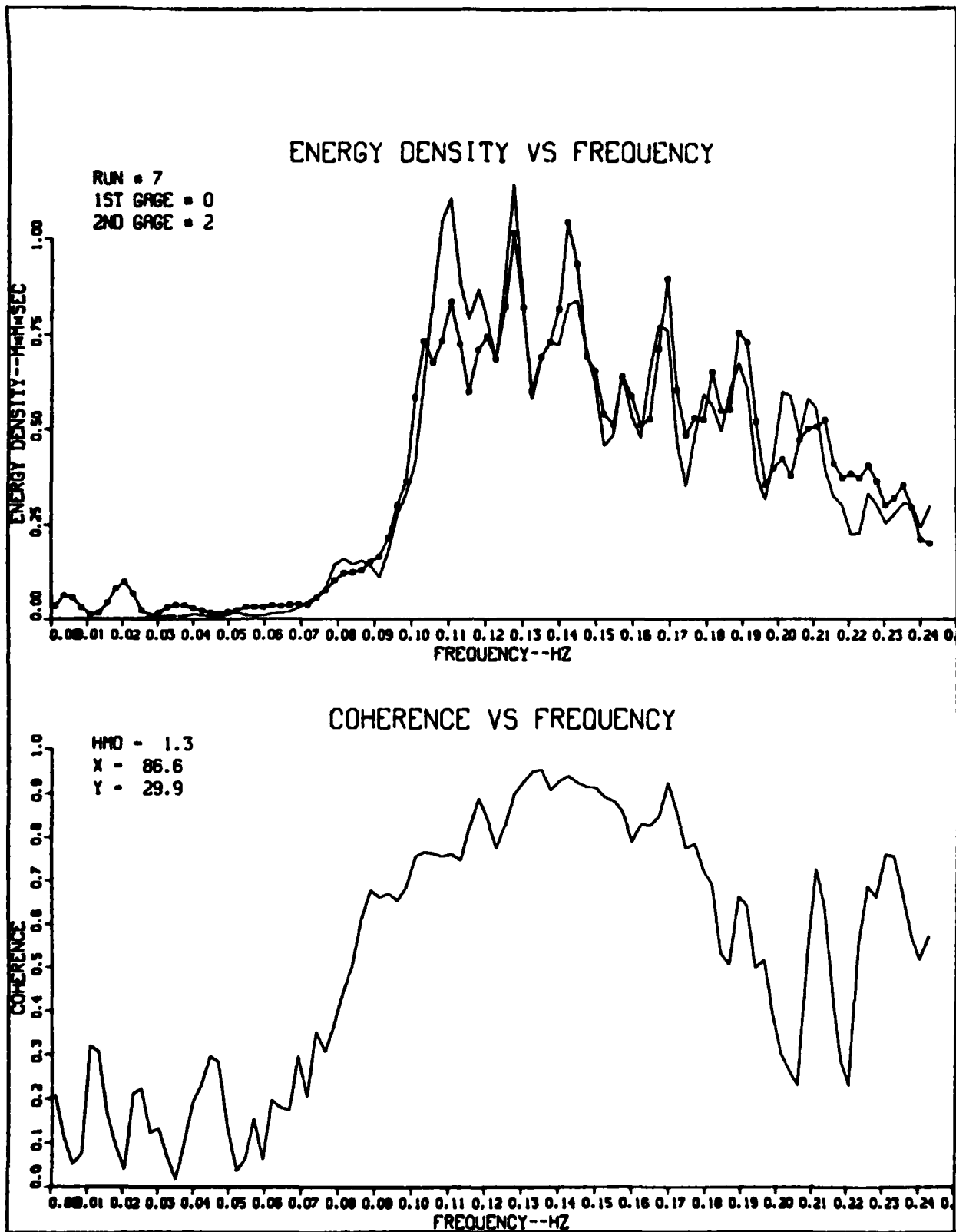


Figure A25. Analysis run 7 of gages 0 and 2

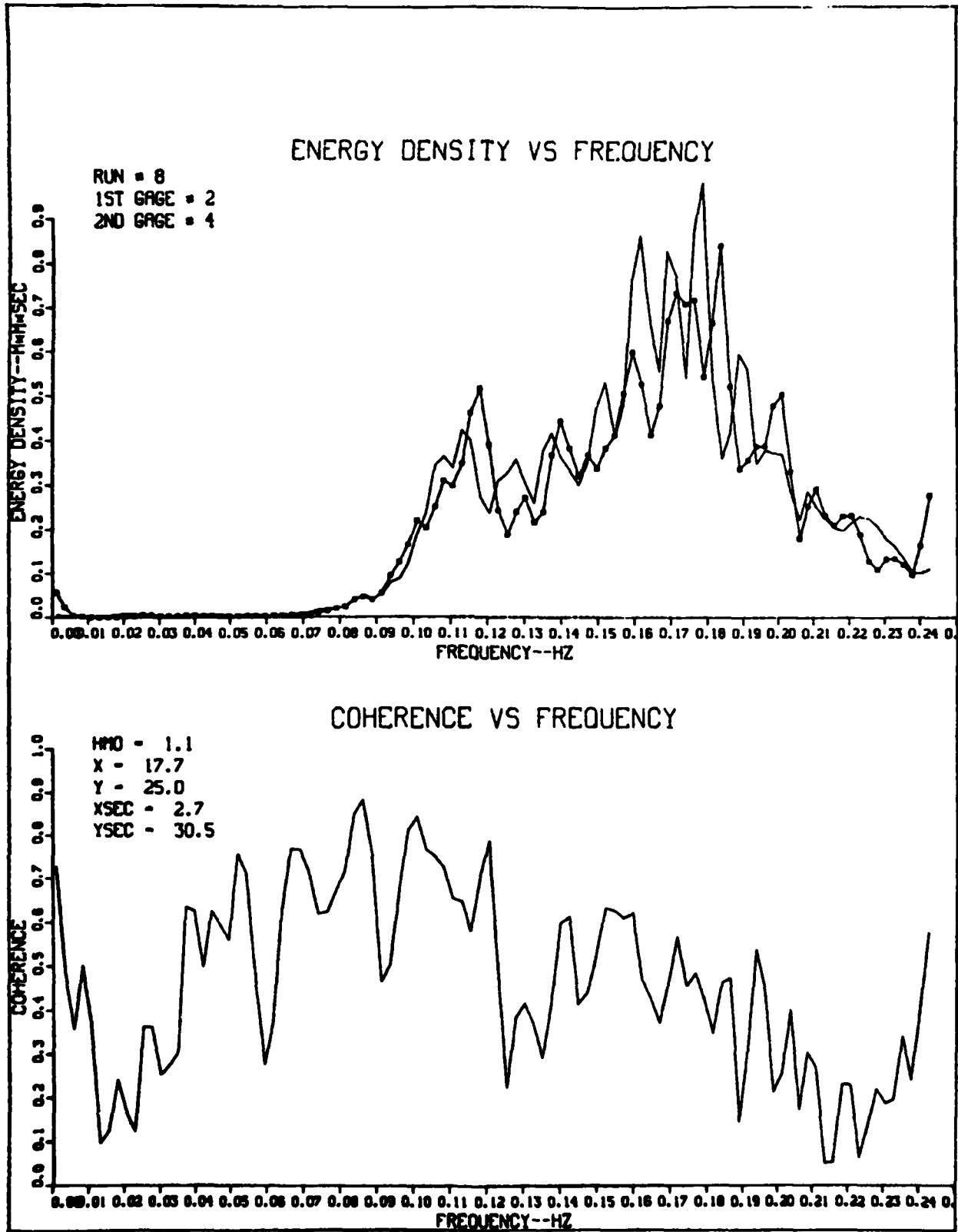


Figure A26. Analysis run 8 of gages 2 and 4

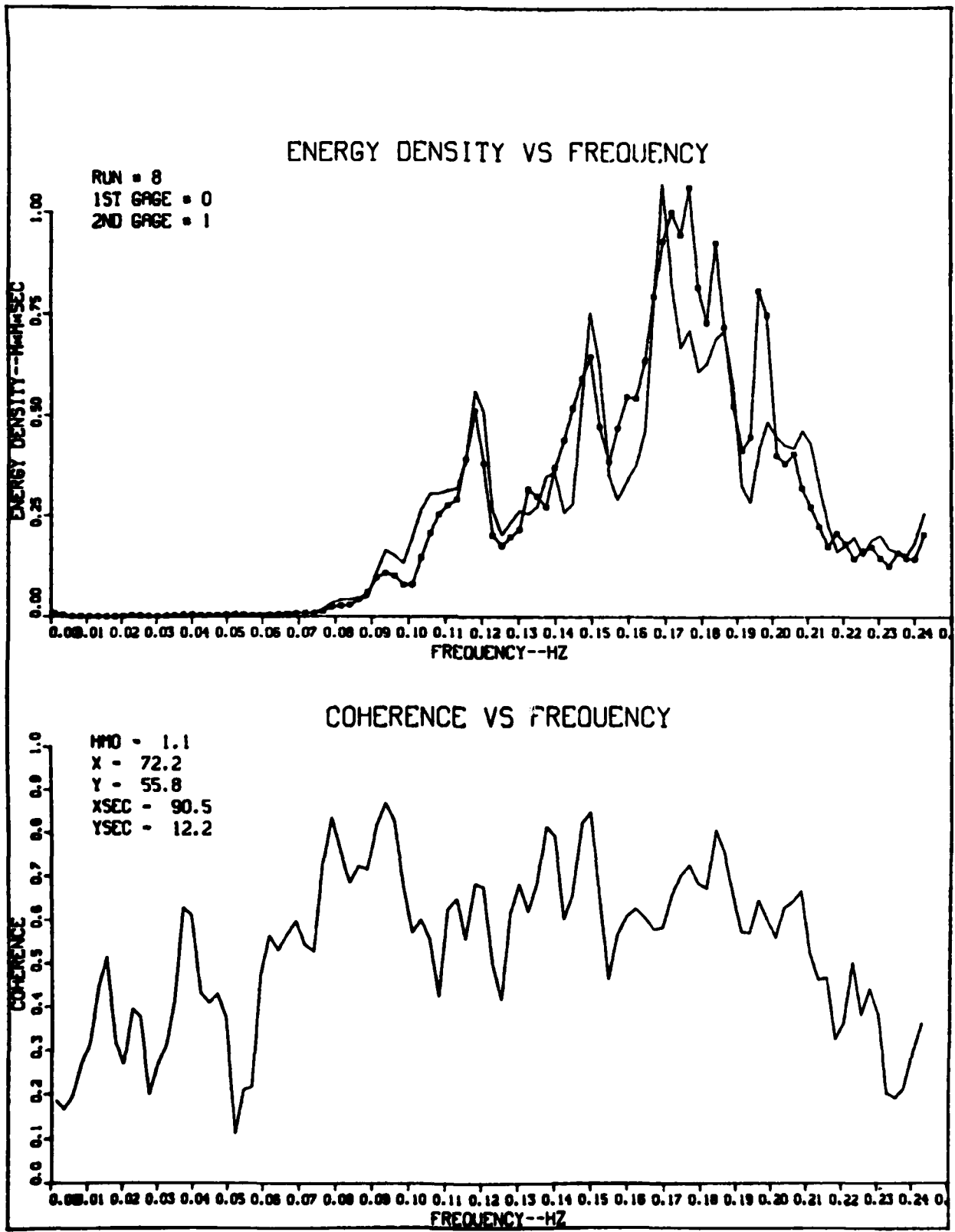


Figure A27. Analysis run 8 of gages 0 and 1

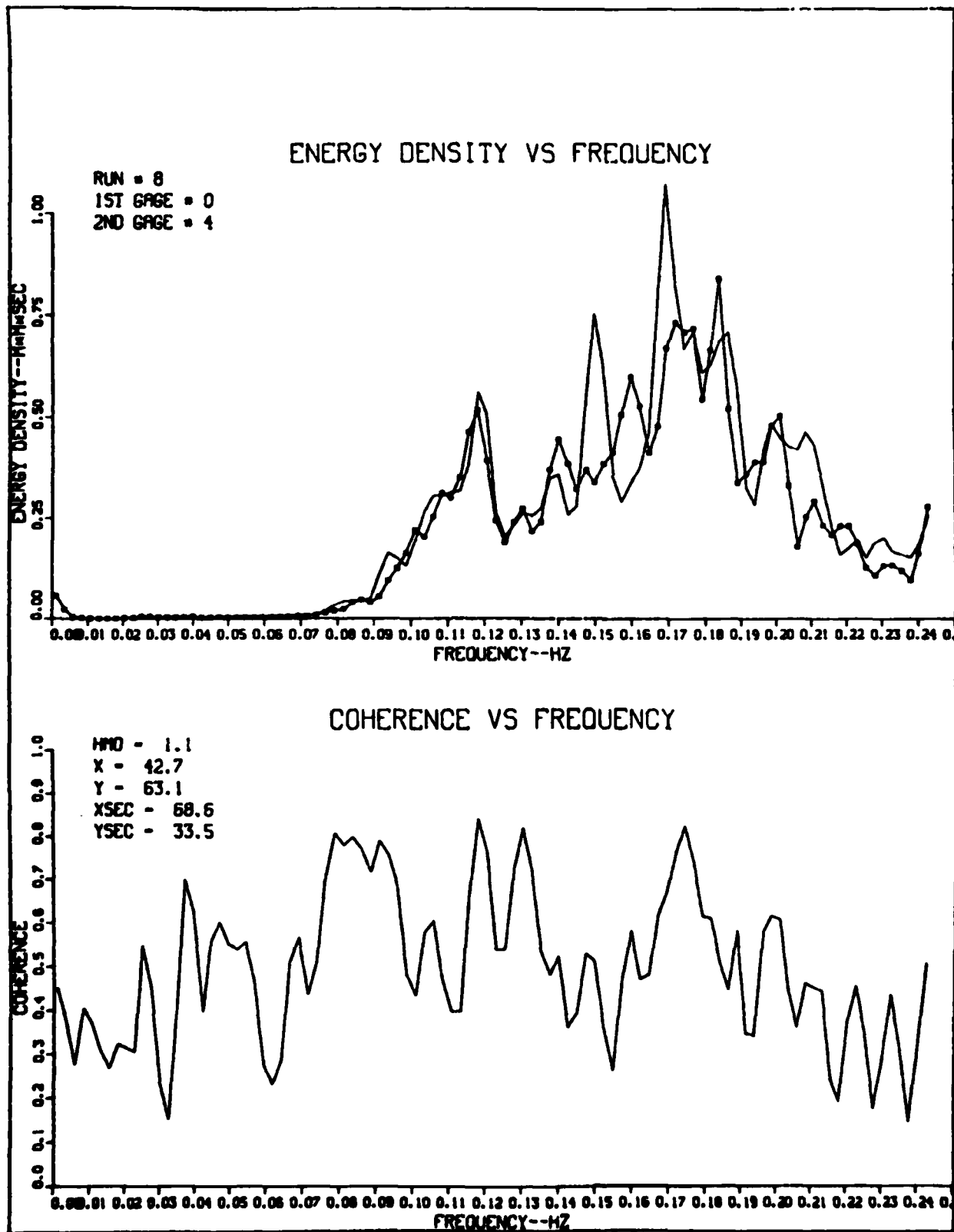


Figure A28. Analysis run 8 of gages 0 and 4

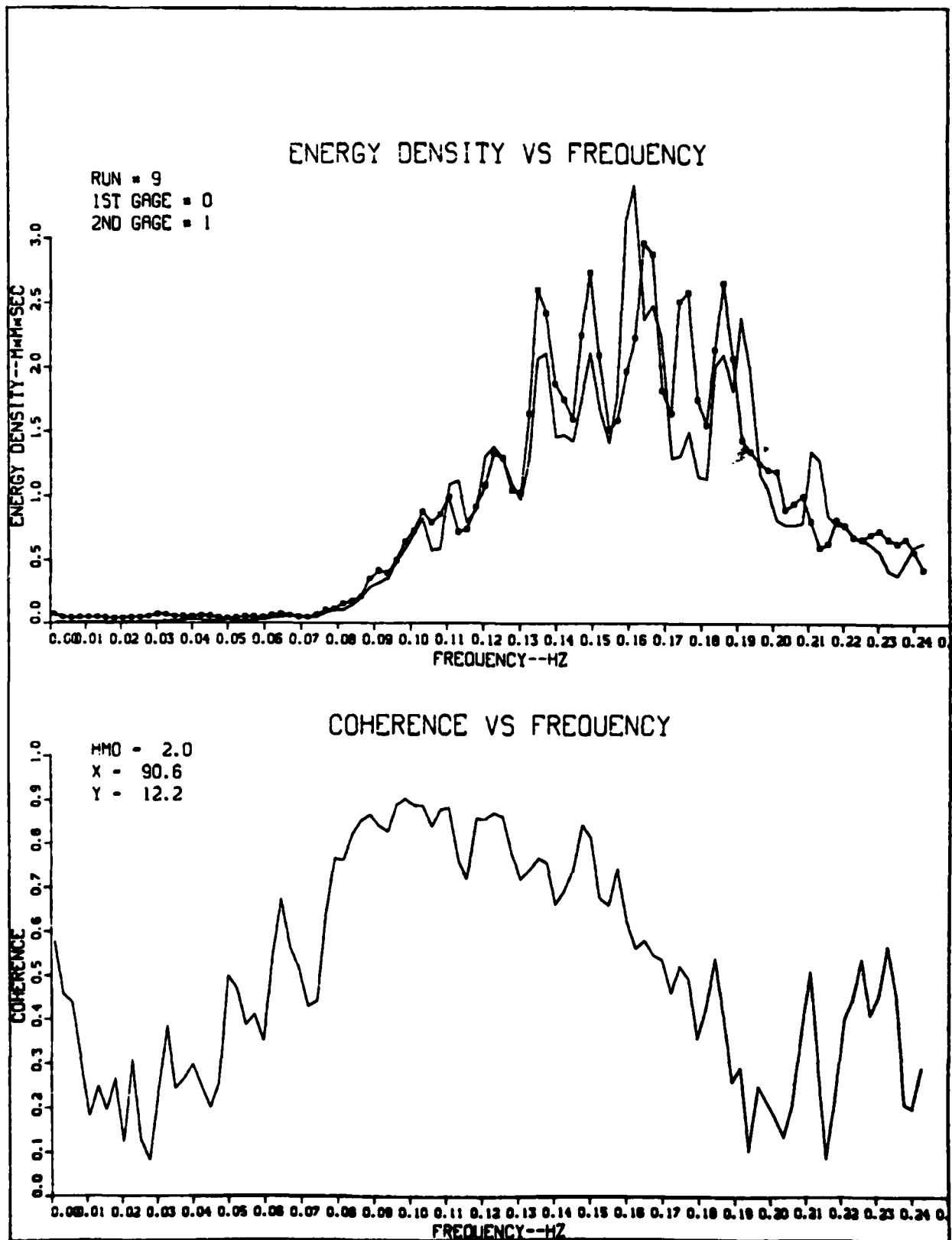


Figure A29. Analysis run 9 of gages 0 and 1

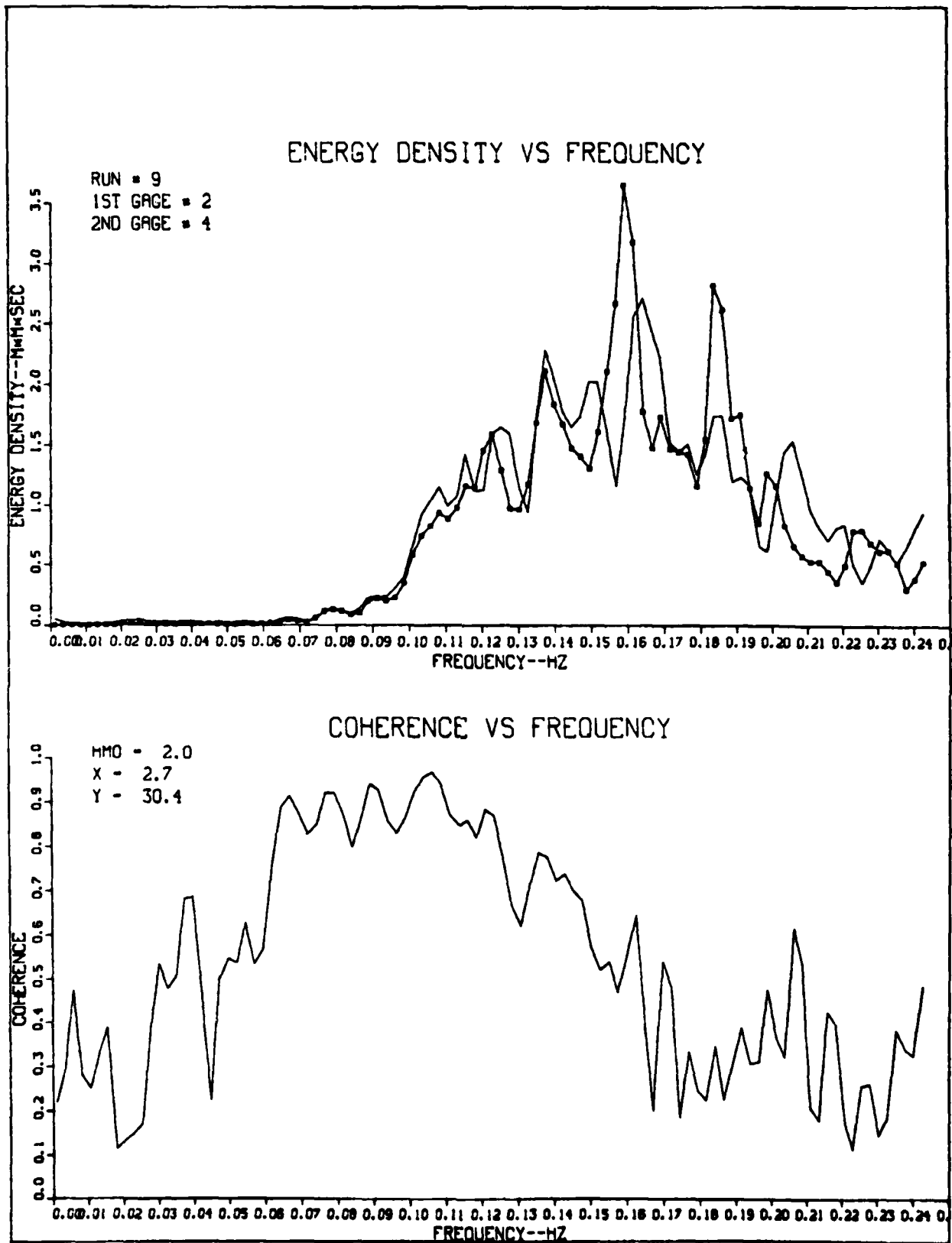


Figure A30. Analysis run 9 of gages 2 and 4

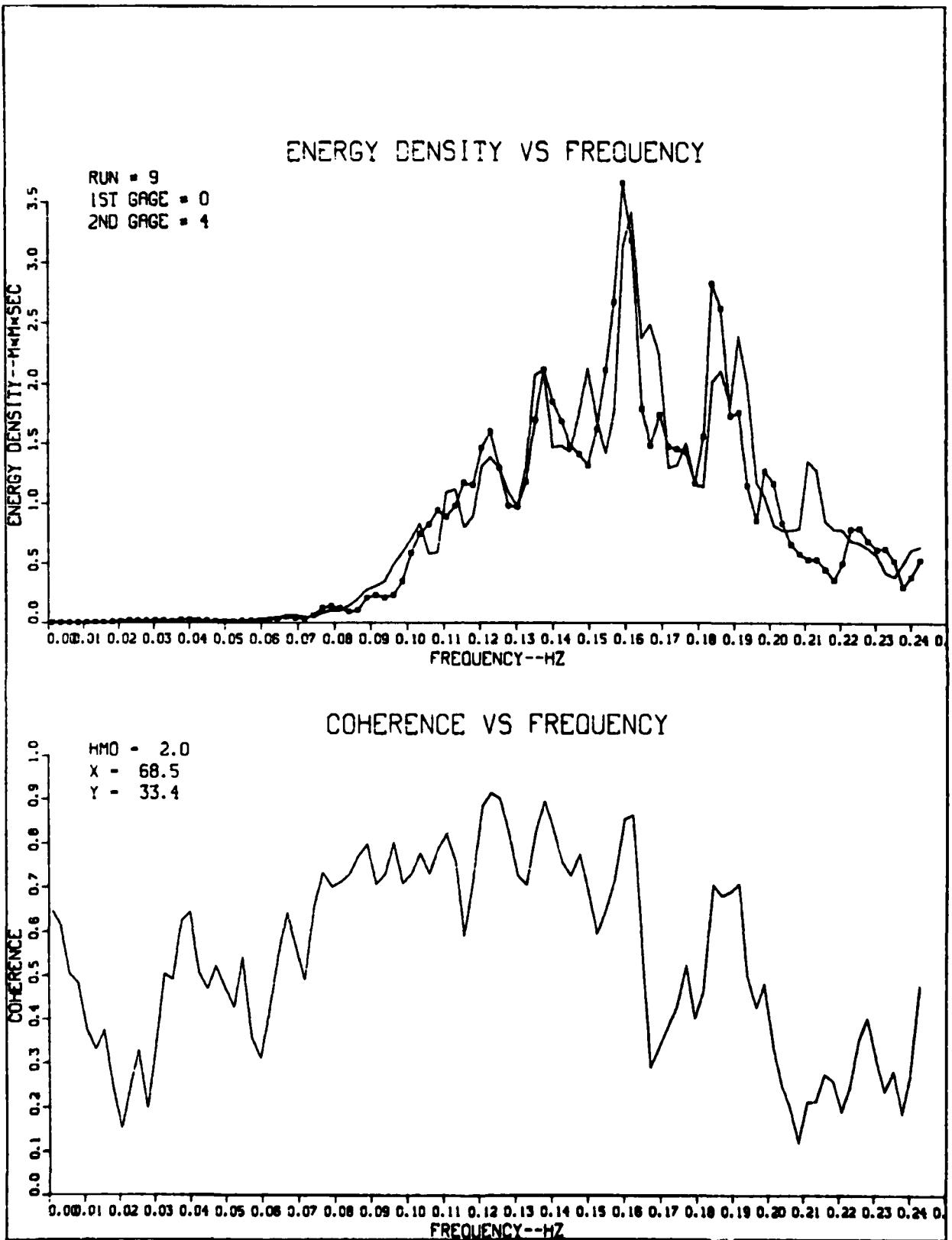


Figure A31. Analysis run 9 of gages 0 and 4

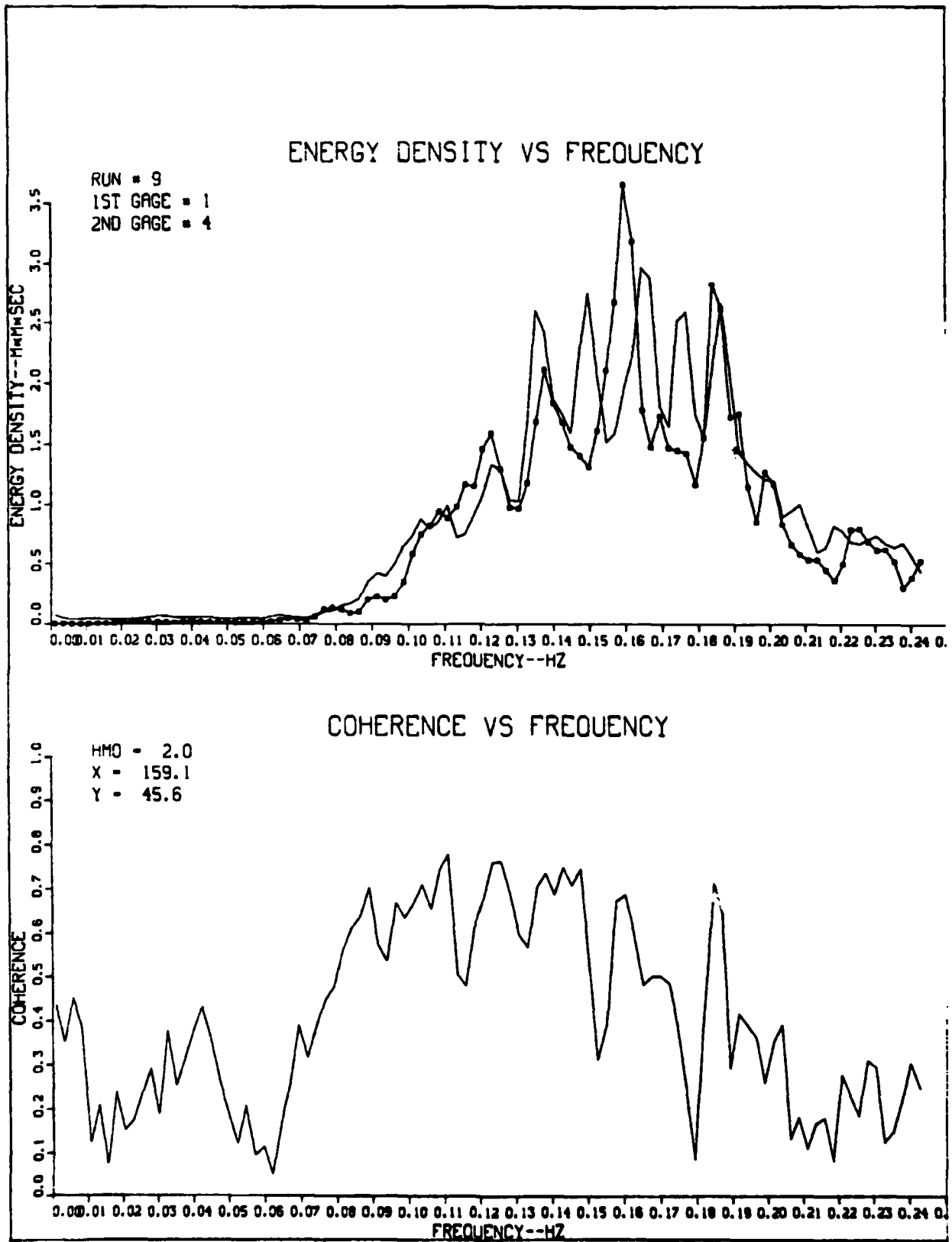


Figure A32. Analysis run 9 of gages 1 and 4

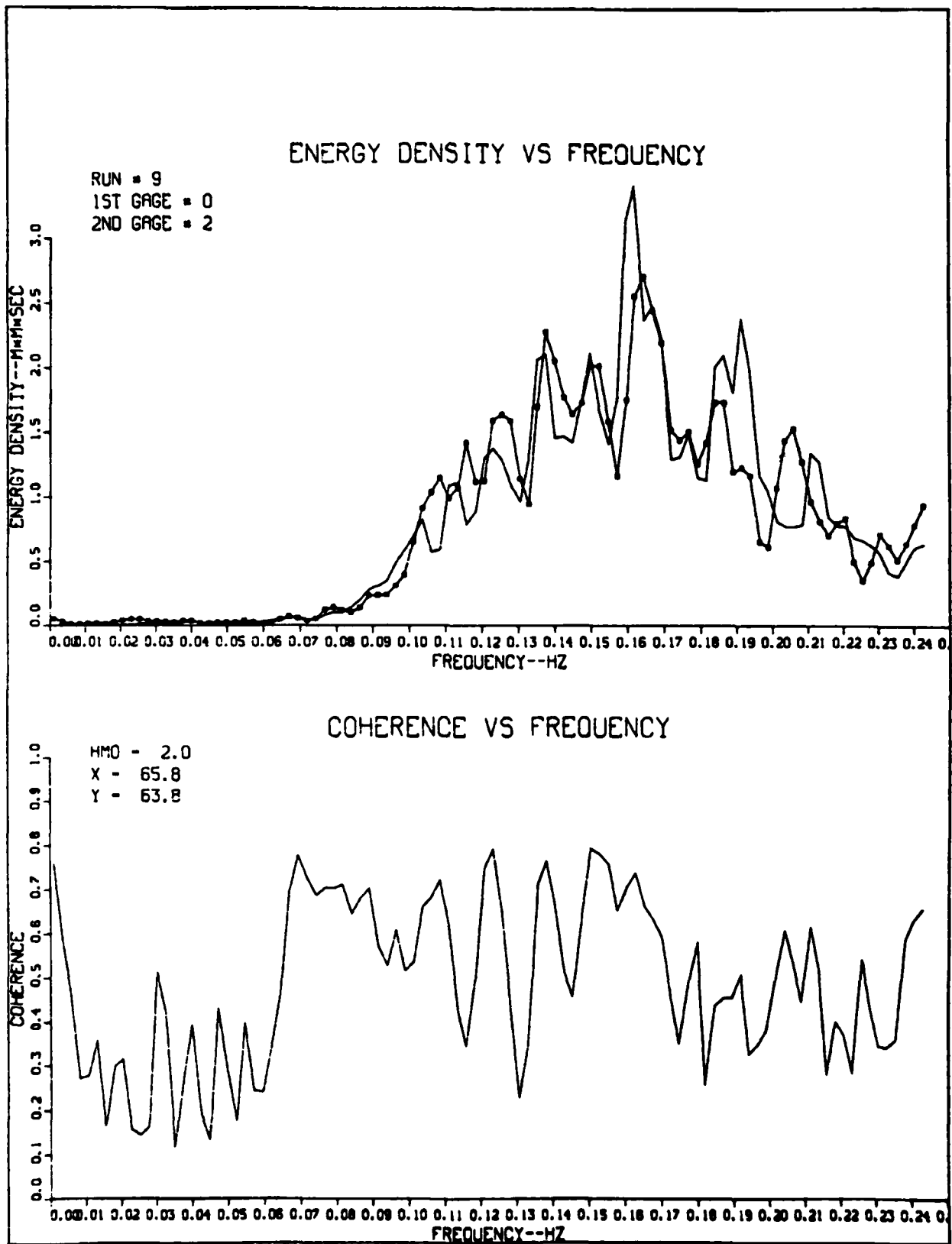


Figure A33. Analysis run 9 of gages 0 and 2

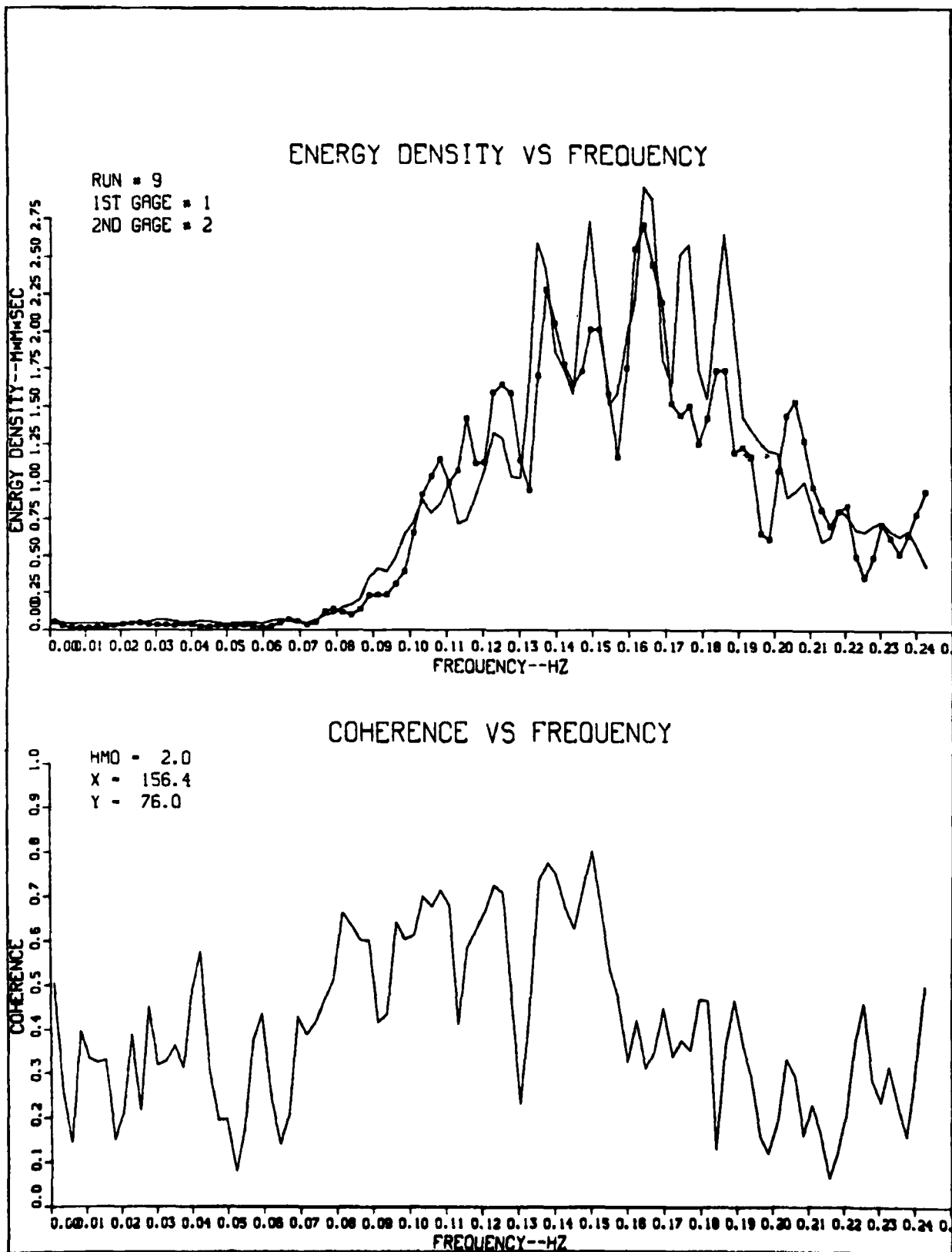


Figure A34. Analysis run 9 of gages 1 and 2

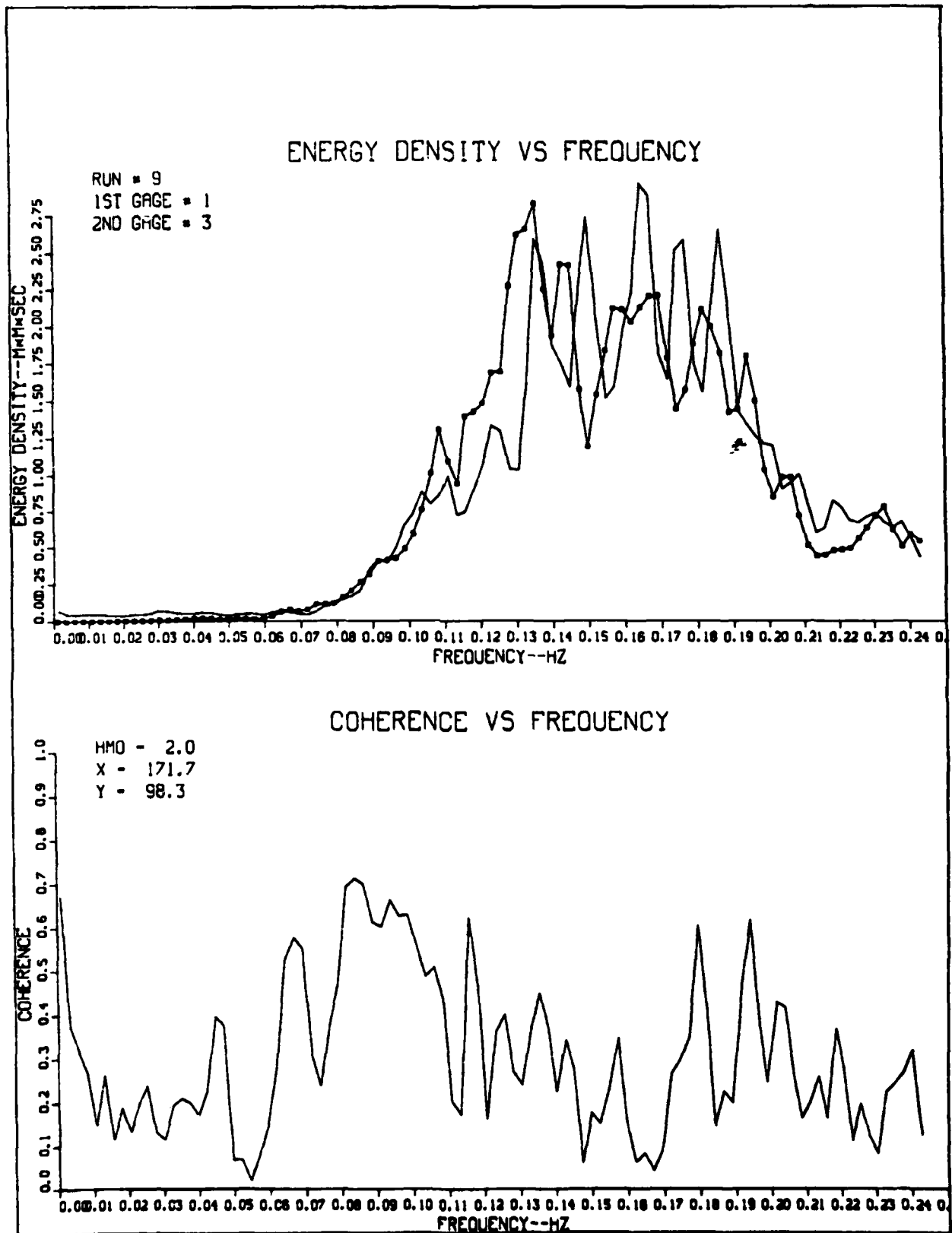


Figure A35. Analysis run 9 of gages 1 and 3

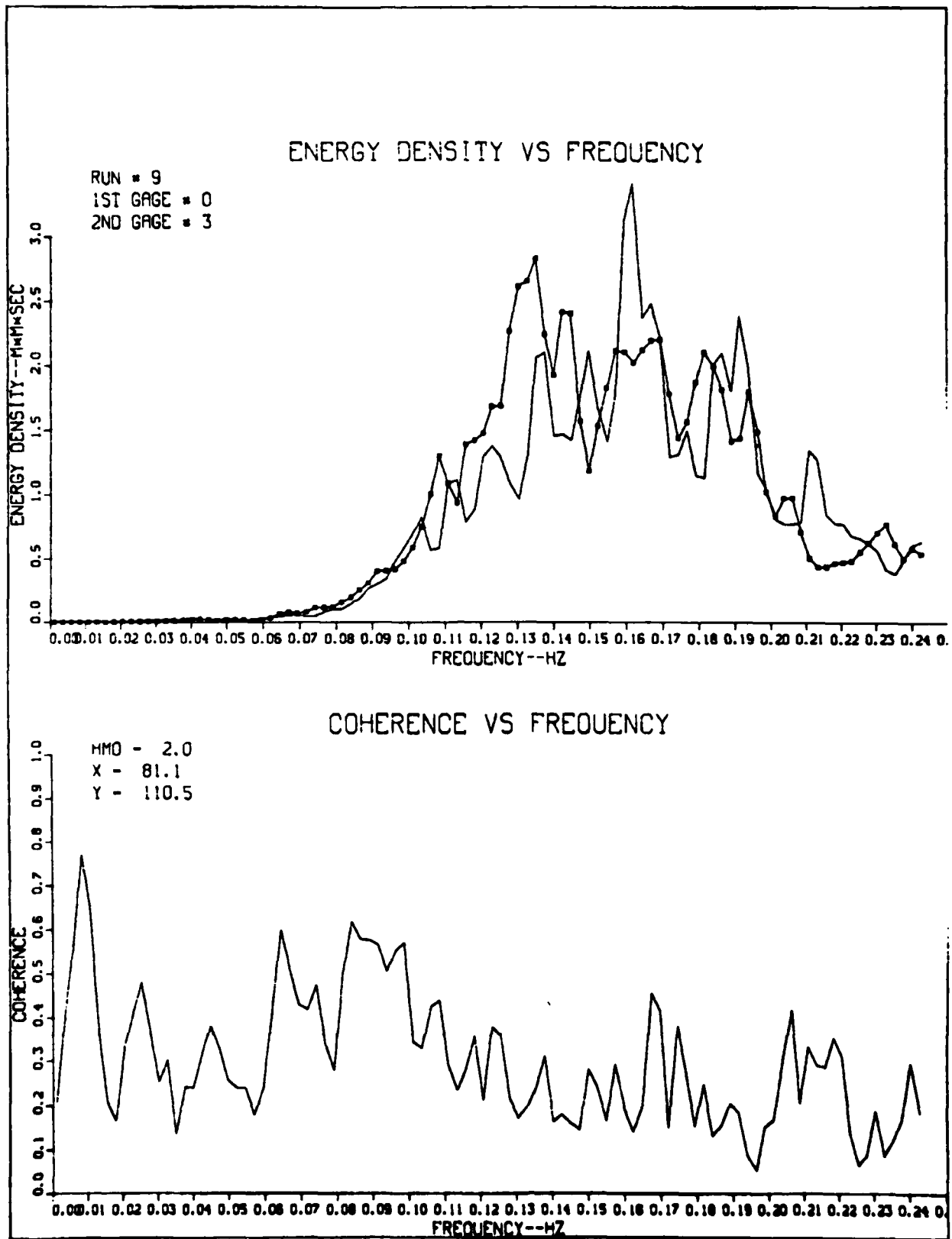


Figure A36. Analysis run 9 of gages 0 and 3

END

FILMED

11-84

DTIC